O. Schlömer[1], and J. Herget[1]

[1]Department of Geography, University of Bonn, Germany

Corresponding author: Oliver Schlömer (oschloem@uni-bonn.de)

Key Points:

- Local scouring at a boulder-like obstacle occurs predominantly on the rising limb when the obstacle is unsubmerged
- Up to 80 percent of the final scour hole size attained in less than 10 percent of hydrograph duration, irrespective of hydrograph shape
- For subsequent hydrographs the dependence on antecedent sizes of the local scour is important which is referred as memory effects

Abstract

Local scouring is a bed load transport phenomenon related to different scientific disciplines in Earth-science and hydraulic engineering. However, less attention is given on the enlargement processes of local scour holes at natural instream obstacles like boulders that are exposed to unsteady flow conditions in the course of a flood hydrograph. Experimental investigations in laboratory flumes offer the advantage that hydraulic boundary conditions can be systematically varied. This contribution yields novel experimental data on the impact of submergence ratio, hydrograph skewness, and flow intensity onto local scour holes at boulder-like obstacles and evaluates the effect of discharge chronologies, i.e. subsequent hydrographs in time onto the geometry of local scour holes. In total 48 unscaled flume experiments for subcritical, clear-water and live-bed conditions were performed. Experimental results reveal that (i) local scouring dominantly occurred at the rising limb when flow depth is comparable to the obstacle size so that the obstacle is unsubmerged. (ii) Up to 80% of the scour hole size at the end of experimental runs was reached in only 10% of the experimental runtime while the skewness of the hydrograph is important. The steeper the rising limb the quicker the local scour hole matured. (iii) Local scouring is history dependent and memory effects are present that describe the dependence on antecedent sizes of the scour hole. It is speculated that speculate that local scour holes found at boulders in the field may be used for the interpretation of the minimum duration of the beginning stage of a flood.

Plain Language Summary

Local scour holes are crescentic depression related to obstruction like natural boulders or artificial bridge piers that are exposed to flowing water. Commonly, local scouring is investigated in flumes that simplify natural conditions. As opposed to bridge piers, boulders are unsubmerged or submerged depending on flow depth which is typically varying during a flood. Here we present the results of an experimental campaign studying local scouring at a boulder-like obstacle that is exposed to laboratory floods. The floods had different duration and intensity and were repeated to evaluate the impact of subsequent flooding

onto local scour holes. The results reveal that local scouring at boulder-like obstacles is very dynamic during the beginning stage of the flood for flow depths that are comparable to the size of the boulder. The peak of a flood had only a negligible impact on local scouring as the boulder-like obstacle was deeply underwater. Local scouring for subsequent floods depends on the antecedent size of the scour hole before the following flood. We speculate that local scour holes found at boulders in the field may be used for the interpretation of the minimum duration of the beginning stage of a flood.

1 Introduction

Local scour holes are crescentic depressions formed by flow separation and local acceleration in the vicinity of an instream obstacle that induce sediment mobilization (Richardson, 1968; Allen 1984). The unique aspect about local scour holes is that they can develop even when the threshold for general sediment movement is not exceeded and clear-water conditions prevail. Due to the variety of natural (i.e. solitary boulders, deadwood) and technical obstructions (i.e. bridge piers, spur dikes, pipelines) the local scouring phenomenon is relevant to different scientific disciplines in Earth-science and hydraulic engineering. Local scouring can be interpreted as the result of a complex two-phase flow involving water and sediment that is controlled by different environmental boundary conditions comprising (1) flow conditions, (2) sediment characteristics, (3) properties of the obstacle, and (4) time (Breusers & Raudkivi 1991; Radice et al. 2009, Schlömer et al. 2020). Hence, laboratory flumes offer the advantage to investigate local scouring by systematically varying boundary conditions and evaluate their impact onto local scour hole geometry and flow structures.

Local scour holes related to natural topographic obstructions exposed to a current are described for a range of conditions, including overland flow at rock fragments (Poesen et al., 1994, Jomaa et al., 2012) and solitary boulders in ephemeral streams with a diameter greater than the mean diameter of the surrounding alluvium (Karcz, 1972, Euler et al., 2017). The boulders are mobile in the sense that they are mobilized as bedload only during extreme magnitude floods (Shobe et al., 2021). However, for typical floods the boulders have to be considered immobile obstacles that are not transported further downstream and remain part of the river landscape (Calle et al., 2017). Thus, in ephemeral dryland streams preserved scour holes are common features at boulders (Reid et al. 1998; Powell 2009) (Figure 1a). Under these conditions local scouring is impacted by the occurrence of flash floods, i.e. a flow of water that arrives suddenly at a fixed point, changes rapidly in velocity and flow depth, and lasts a short time (cf. Alexander & Crooker, 2016). Herget et al. (2013) used the preserved geometry of local scour holes at large boulders located in arid and ungauged basins to estimate flow velocities of past flood events. Although plausible results could be presented, the spatio-temporal evolution of local scour hole at boulder-like obstacles during a flood event is not systematically investigated yet. Thus, present experimental methods neglect four important properties:

1. Natural floods are characterized by unsteady discharge (i.e. velocity and

flow depth at any fixed point in space varying over time) that causes different flow depths at the obstacle.

2. Unsteady discharge is characterized by hydrographs for which the duration of the rising limb relative to the falling limb describes the hydrograph's skewness (Herget et al., 2015, Collischonn et al., 2017) that affects local scouring in time.

3. For peak flow the flow intensity (i.e. mean approach flow velocity relative to threshold velocity for general sediment movement) might be greater than 1 so that live-bed conditions (i.e. general sediment transport in the upstream flow) prevail which result in refilling mechanisms of the emerging scour hole

4. Local scouring is not independent from past flood events and accumulating due to subsequent flood events, known as memory effect (Tubaldi et al., 2017, Pizarro & Tubaldi, 2019).

Immobile boulders are also often used in river restoration practices to enhance habitat quality in degraded rivers that cause a higher variability in flow structures (Fisher & Klingman, 1984). From prior laboratory research on flow structures at boulders it is know that submergence ratio (ratio of approaching flow depth to size of the obstacle) is a particularly important boundary condition (Boyer & Roy, 1991; Shamloo et al., 2001; Papanicolaou et al., 2010; Euler et al., 2017). During lower flows, the obstacle is unsubmerged (some portion of the obstacle protrudes above the water surface) and the flow might be affected by localized flow structures (e.g. hydraulic jumps) as it becomes a function of Froude number. Whereas at higher flow, the obstacle occupies only the lower portion of the flow depth and the obstacle is submerged and the flow is subcritical.

From laboratory research on unsubmerged bridge piers (Melville & Coleman, 2000, Ettema et al. 2011; Pizarro et al. 2020) and submerged pipelines (Sumer and Fredsøe, 2005) it is known that local scouring is non-linear in time and approaches an equilibrium condition, defined based on the maximum depth of the local scour hole that is likely after prolonged exposure to steady flow. For non-cohesive alluvial sediment (i.e. sand and gravel) equilibrium conditions are typically reached in order of days (Kothyari et al. 1992a; Simarro et al. 2011; Oliveto & Hager 2002). However, it is well established that for steady discharge 80% of the local scour hole size at equilibrium condition is reached within only 5-40% of the time to equilibrium mainly depending on flow velocity and grain size (Melville & Chiew 1999). In course of unsteady discharge, experimental studies on bridge pier scouring found that that the rising limb and peak flow have the strongest impact onto local and that the time to reach maximum scour depth is usually smaller than the flood duration (Link et al., 2017, 2020, Pizarro et al., 2017; Bombar, 2020).

However, the temporal evolution of local scour holes at boulder-like obstacles affected by different water levels in course of a flood event is not experimentally investigated yet. Thus, the present study experimentally investigates the

impact of hydrographs of different skewness, varying water levels at the obstacle, varying duration, and different flow intensity onto enlargement processes of local scour holes at boulder-like obstacles in time. Furthermore, the effect of subsequent flood events is considered. Within this context, the objectives of the contribution are:

1. Present experimental data on the enlargement of local scour holes at boulder-like obstacles in time that are exposed to different water levels.
2. Analyze the geometry of local scour holes for unsteady discharge in time by a systematic laboratory flume study.
3. Evaluate the history-dependence of local scouring at boulder-like obstructions for different hydrograph scenarios.

The study uses process-focused laboratory prototypes (Baynes et al. 2018) that reproduce processes and resulting morphologies (i.e. scour holes). The hydrographs were constructed to represent hydraulic conditions in ephemeral dryland streams, but do not represent a specific natural prototype. Hydrographs were operationalized upon dimensional parameters. The time-series data on local scour hole geometry were utilized by statistical and regression analysis.

1.1. Processes of Local Scouring at Boulder-Like Obstacles

If the boulder is unsubmerged which is a condition analogously to scouring at bridge piers, the following processes are common (1) increased flow velocity lateral to the obstacle; (2) formation of a jet-like downflow at the obstacle front due to pressure gradient; (3) formation of unsteady turbulent necklace-like vortical structures at the obstacle base commonly referred as horseshoe vortex system (HV) (Escauriaza & Sotiropoulos 2011; Kirkil & Constantinescu 2010; Radice & Tran 2012; Chen et al. 2017). Processes (1) to (3) amplify bed shear stress and induce sediment mobilization (Li et al. 2018; Link et al. 2012). However, boulders have to be considered as relatively squat (height $<$ width) at all flow depths and it is likely that the boulder gets submerged during a flood event while additional vortical structures become dominant. For these conditions, an arch-shaped vortex (Okamoto & Sunabashiri, 1992, Pattenden et al., 2005) is present due to flow separation at the obstacle, compound of two lateral vortices at the obstacle's sides, and a vortex located at the crest of the obstacle (Shamloo, 2001, Dey et al., 2011, Haijmirazie et al., 2014). The arch-vortex bends down to the bed immediately downstream of the boulder (i.e. near-wake) and causes a recirculation zone where some part of the flow reverses towards the obstacle (Euler & Herget, 2012, Papanicolaou et al., 2012) A shown by Euler et al. (2017) and Schlömer et al. (2020) this recirculation zone can cause local scouring in the obstacle's wake instead of frontal local scouring. Thus, the size and the shape of the boulder are of paramount importance for scouring processes. The effective size of the boulder can be described based on height above streambed and width as size perpendicular to the direction of flow. Additionally, the length of the obstacle in stream-wise direction is important as it defines the hydrodynamic shape, generally differing between

streamlined obstructions with cross-flow dimensions smaller than its stream-wise dimensions and bluff obstructions with cross-flow dimensions comparable to its stream-wise dimensions (e.g. Douglas et al., 2001). Generally, local scouring at the obstacle front is more intense for bluff obstructions. Moreover, boulders in streams are mobile in the sense that scouring can undermine the obstacle and induce movement that is characterized by tilting and self-burial of the obstacle once a critical depth of scouring is crossed (Friedrichs et al., 2016, Rennie et al., 2017). Consequently, this process changes the boulder's exposure to flow and alters scouring processes.

1.2. Geometry of Local Scour Holes

A macroscopic pattern of the scour hole at boulder-like obstacles is identified that is consistent over a range of spatial scales from small scale laboratory (10^{-2} m) to scour holes at boulders (10^{1} m) (Schlömer et al., 2021) (Figure 1). Local scour holes can be approximated as inverted frustum-cone with an elliptical shape in plan-view (Figure 1c). The geometry of the scour hole can be characterized by certain geometrical length scales, including scour hole depth at the obstacle front (d_s) measured from the undisturbed upstream bed; scour hole frontal length (l_s) in the plane of symmetry to the incoming flow, measured from the obstacle frontal face to the upstream edge of the scour hole, and scour hole frontal width (w_s) measured perpendicular to the direction of incoming flow form the lateral edges of the scour hole at the obstacle frontal face (Euler & Herget, 2012).

The enlargement of the sour hole and its geometry are closely related to the HV as the main driver of sediment mobilization (Dargahi 1990, Chen et al. 2019). Within the scour the HV actually consists of several interacting and unsteady vortices (Kirkil et al., 2008; Chen et al., 2017). The largest and most stable vortex is denoted as the primary horseshoe vortex (HV1) which is located close to the obstacle base. Upstream, a smaller and less coherent vortex (HV2) is located within the outer region of the frontal scour hole. The vortices are responsible for the segmentation of the longitudinal scour slope, originating from the obstacle front to the upstream edge of the scour hole (Figure 1d). These segments consist of: (1) a flat semi-circular scour hole bottom (Sb) that is closely attached to the obstacle base with radius $< l_s$, (2) an inner frontal scour hole (lower slope) that is characterized by an inclination (Φ) critical angle of repose (Φ_{crit}), and (3) an outer frontal scour hole (upper slope) that is characterized by Φ Φ_{crit}.

The inner scour hole is shaped by the rotation of the HV1 that generally stabilizes the lower slope in an angle greater than the angle of repose (Muzzammil and Gangadhariah, 2003; Unger and Hager, 2007). A knickpoint in the slopes (i.e. berm) differentiates inner and outer scour hole. However, as recently demonstrated by Guan et al. (2019) the HV is an unsteady vortex system that randomly oscillates in time, and thereby temporarily weakens due to aperiodic bimodal oscillations. This changes the position and shape of the vortex core in relation to the obstacle (Paik et al., 2007; Kirkil and Constantinescu, 2015).

During scouring HV1 sinks into the frontal scour hole and extends down to S_b. The enlargement of l_s and w_s is directly related to deepening and occasionally weakening of the HV that destabilizes the scour slopes and results in gravity mass movements.

Contrary to the dominant morphology, local scour holes in the wake of boulders located in high-gradient step-pool streams (Comiti et al., 2005, Polvi 2021) and rock sills (e.g. Pagliara & Palermo, 2008, 2018) are reported. This plunge pool scour occurs as a result of an overtopping jet-stream motion that differs from the HV-induced processes.

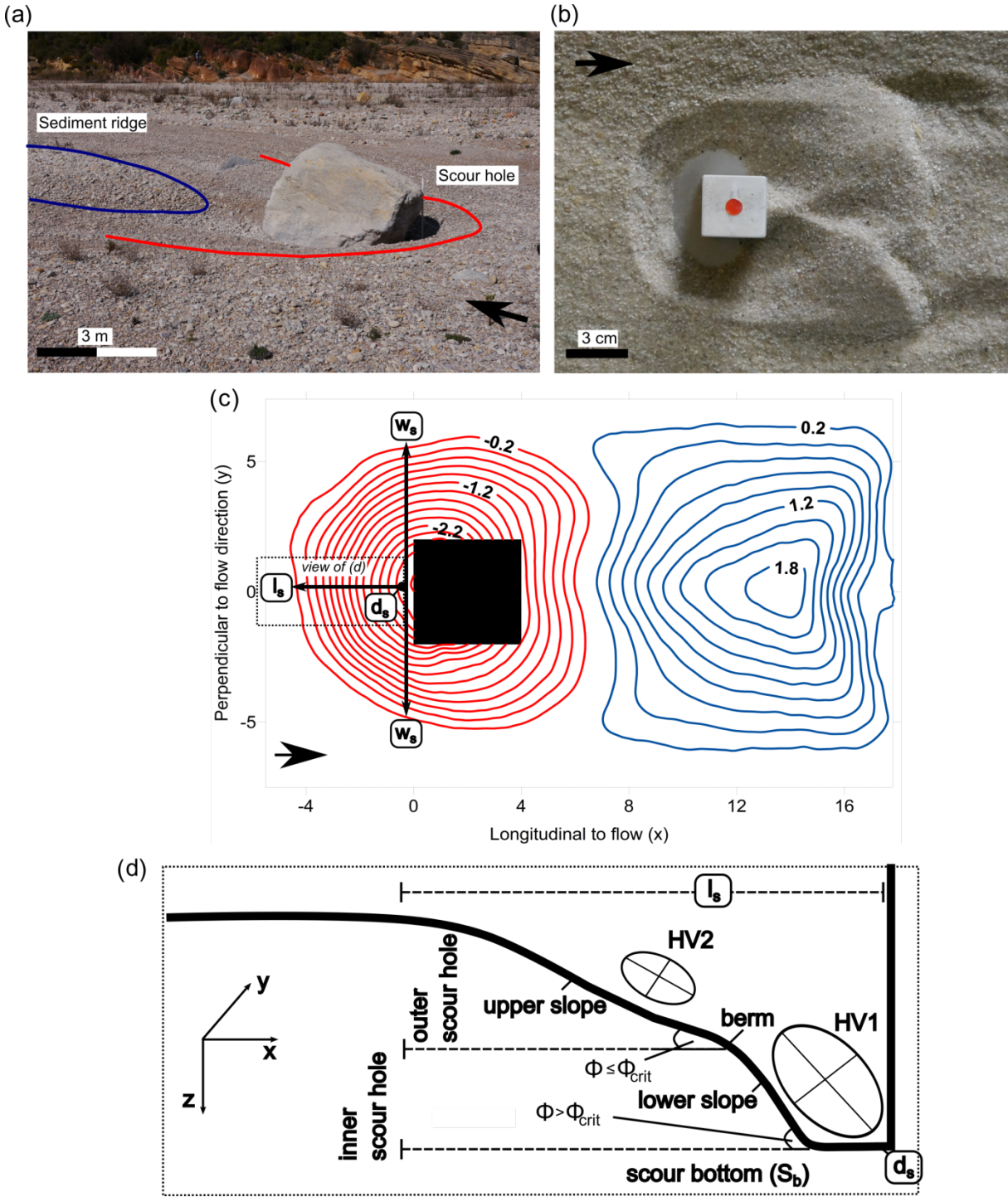
(a)
Sediment ridge
Scour hole
3 m
(b)
3 cm
(c)
w_s
-0.2
-1.2
-2.2
0.2
1.2
1.8
view of (d)
l_s
d_s
Perpendicular to flow direction (y)
5
0
-5
-4
0
4
8
12
16
Longitudinal to flow (x)
(d)
l_s
HV2
outer scour hole
upper slope
berm
HV1
y
x
z
$\Phi \leq \Phi_{crit}$
lower slope
$\Phi > \Phi_{crit}$
inner scour hole
scour bottom (S_b)
d_s

Figure 1. (a) Local scour hole at a boulder in ephemeral Rambla de la Viuda (2019, NE Spain) at field scale (m).(b) Local scour hole at a cube generated in a flume at laboratory scale (cm).(c) Plan view of a local scour hole at a cuboid obstacle at laboratory scale (cm) indicating local scour hole (red isolines) and sediment ridge (blue isolines). (d) Upstream cross-sectional profile of the frontal scour hole indicating internal differentiation and positions of primary horseshoe vortex (HV1) and secondary horseshoe vortex (HV2), (not to scale). Arrows indicate direction of flow. (c) and (d) are reproduced from Schlömer et al., (2021).

1.3. Boundary Conditions of Local Scouring at Boulder-Like Obstacles

Local scouring at a solitary solid boulder-like obstructions located in a straight, moderately sloped channel with subcritical (Fr < 1) flow conditions and cohesion less alluvial sediment (i.e. plane-bed type streams, Simons and Richardson 1966) can be functionally determined by:

$d_s = f\ (d_w, U_m, \ , \ , g, B, h_o, w_o, le_o, Mb, D_{50}, \ _s, \ _G, U_c, d_{sed}, t)$ [Eq. 1]

where d_s is local scour depth [L], d_w is flow depth [L], is water density [ML^{-3}], is kinematic viscosity [L^2T^{-1}], g is gravitational acceleration [LT^{-2}], B is channel cross section [L], h_o is height of the obstacle [L], w_o is obstacle width [L], le_o is length of obstacle [L], Mb is an indicator for the mobility of an boulder-like obstruction, due to tilting into the scoured depression [-], D_{50} is median grain diameter of the bed sediment [L], $_s$ is sediment density [ML^{-3}], $_G$ is gradation coefficient of sediment ($D_{84}/D_{16}{}^{1/2}$ [-]), U_c is critical mean approach velocity for entrainment of bed sediment [LT^{-1}], d_{sed} is the thickness of the bed layer [L], and t is time [T].

In Eq. (1), 16 independent variables (denoted n) in 3 basic dimensions (denoted m) define the problem's inherent degrees of freedom (e.g. Sonin, 2004). According to the -theorem (e.g. Barenblatt, 2003) Eq. (1) can be reduced to n - m non-dimensional parameters. To account for squat obstacles at unsubmerged and submerged conditions at the obstacle, obstacle height (h_o) and width (w_o) are used to define the effective obstacle size ($L_o = h_o \ w_o \ = h_o{}^{2/3} \ w_o{}^{1/3}$), with $+ \ = 1$. L_o is used as a reference length scale [L] while the exponents were derived from a data analysis presented in Euler and Herget (2011) and Oliveto and Hager (2002). Assuming constant relative sediment density (s-)/), i.e. neglecting and $_s$ among other expression one get:

$d_s/L_o = f\ (d_w/L_o, U_m/g^*L_o{}^{1/2}, U_m/U_c, U_m{}^*L_o/\ , L_o/B, Sh, Mb, L_o/D_{50}, \ _G, d_{sed}/L_o, t/t_e)$ [Eq. 2]

where d_s/L_o is the non-dimensional scour depth, d_w/L_o is submergence ratio, U_m/U_c is flow intensity, $U_m/g^*L_o{}^{1/2}$ is Obstacle-Froude number (Fr_o), $U_m{}^*L_o/$ is Obstacle-Reynolds number (Re_o), L_o/B is blockage ratio, Sh (L_o/le_o) describes the hydrodynamic shape of a body, for (Sh 0.5) the obstructions is

bluff while for Sh 0.8 the obstacle is more streamlined, L_o/D_{50} is the relative sediment coarseness, d_{sed}/L_o is the relative thickness of the bed layer, with L_o representing the size above the sediment bed (d_{sed}). For $d_{sed}/L_o < 1$ the sediment layer is too thin and ds incision is significantly limited, while slight enlargement of w_s and l_s could be observed (Schlömer et al., 2021). If $d_{sed}/L_o = 0$ the formation of obstacle marks as a sedimentary structure is inhibited. t_e is time scale to reach equilibrium [T] that is a function of d_w/L_o, U_m/U_c and L_o/D_{50} (e.g. Melville and Chiew, 1999).

In order to keep flow intensity (U_m/U_c) as parameter to discern between clear-water ($U_m/U_c < 1$) and live-bed conditions ($U_m/U_c > 1$), Fr_o is excluded (cf. Simarro et al., 2007). Viscous effects are neglected (i.e. Re_o excluded) (Manes et al. 2018, Lanca et al., 2016). The following parameters were kept constant during experiments: $L_o/D_{50} = 40$, $L_o/B = 0.09$, $_G < 1.3$, $d_{sed}/L_o > 1$, $d_{sed}/L_o > 1$, thus Eq. (2) reduces to:

$d_s/L_o = f\ (d_w/L_o, U_m/U_c, t/t_e)$ [Eq. 3]

Due to shape similitude of the scour hole (Schlömer et al., 2021, Euler et al, 2017) and the dependence of scour hole width and length enlargement on scour hole depth, d_s/L_o can be replaced by l_s/L_o or w_s/L_o while d_s/L_o can substitute any of the non-dimensional parameters on the right side of Eq. (3) (Chreties et al., 2008):

$w_s/L_o = f\ (d_w/L_o, d_s/L_o, t/t_e)$ [Eq. 4]

$l_s/L_o = f\ (d_w/L_o, d_s/L_o, t/t_e)$ [Eq. 5]

While Equation (3) applies for steady flow, Pizarro et al., (2017) proposed the dimensionless effective flow work (W*) as generalization of the flow intensity concept to unsteady flow conditions which integrates effects of hydrograph shape, peak flow and duration onto local scouring at unsubmerged obstacles (i.e. bridge piers):

$W^* = \int_0^{t_{end}} \frac{1}{t_e}(\frac{U_m}{U_c} - 0.5)^3 \delta dt$ [Eq. 6]

where t_{end} is the hydrograph duration and is delta Dirac function:

$$\delta \begin{cases} 0 \frac{U_m}{U_c} < 0.5 \\ 1 \frac{U_m}{U_c} \geq 0.5 \end{cases} \quad \text{[Eq. 7]}$$

Integrating W* in further analysis reduces Eq. (3) to:

$d_s/L_o = f\ (d_w/L_o, W^*)$ [Eq. 8]

while Link et al., (2017) described the relationship between normalized scour hole depth and W* as:

$d_s/L_o = 0.0075*(1\text{-}e^{-0.097\ W^{*\wedge 0.38}})$ [Eq. 9]

According to Pizarro et al., (2017), W* was computed in an approximate and discrete form:

$W^* = \sum_{i=0}^{n} (\frac{U_m}{U_c} - 0.5)^3$ i Δt [Eq. 10]

with Δt is the measuring interval of unsteady discharge and n = t_{end}/ Δt.

U_c was estimated for different d_w by:

$U_c = 5.75_{log10}\ (5.53 d_w/D_{50}) u_{c*}$ [Eq. 11]

where u_{c*} is the critical shear velocity [LT^{-1}] that was estimated by:

$u_{c*} = (0.0115+0.0125) {D_{50}}^{1.4}$ (0.1 mm < D_{50} < 1 mm) (Melville & Coleman, 2000) [Eq.12]

2 Experimental Design

2.1. Flume Setup

Experiments were conducted in a in a 5 m long, 0.32 m wide, and 0.27 m deep straight rectangular flume- entirely filled with a 5.5 cm thick layer (d_{sed}) of uniform ($_G$ < 1.3) sand with median grain diameter (D_{50} = 0.75 mm). D_{16} and D_{84} were 0.61 mm and 0.89 mm, respectively. The critical angle of repose (Φcrit) when dry is estimated ~ 33° (Dey 2014).

A cube (L_o = 3 cm) was used to represent the hydrodynamic shape of a bluff instream obstacle whose cross-flow dimensions are comparable to its stream-wise dimensions. The authors are aware that the shape of a cubic boulder is unlikely for natural conditions. However, the cube is supposed to represent a maximum angular obstacle for which scouring processes are intensified.

The cube was mounted to the flume bottom to prevent tilting due to scouring which limits further evolution of local scouring and induces equilibrium conditions more quickly (Friedrichs et al., 2016, Rennie et al., 2017). The obstacle was installed in the working section of the flume (~ 2.7 m downstream of the inlet) in the plane of symmetry to minimize sidewall effect (Nakagawa & Nezu 1993), (Figure 2a).

Discharge was controlled by a recirculating pump (Lowara FCE-series®) regulated manually by two cone valves and measured by a magnetic-inductive discharge meter (Schwing MS 1000®, accuracy ± 1% of actual discharge). Flow depth (d_w) was adjusted by a tailgate at the downstream end of the flume outlet. In order to reduce turbulence and to condition flow a self-made flow straightener made of bundled pipes (approx. 100 pipes, diameter 3 cm, length 40 cm) was installed in the flume inlet. The water surface profile in the working section (~ 2.7 m downstream of the inlet) was measured using an ultrasonic distance meter (Mic +25, Microsonic®, accuracy ± 0.1 mm). At peak flow d_w was 8 cm while U_m was 0.26 ms^{-1}, 0.32 ms^{-1}, and 0.37ms^{-1}, respectively.

The bottom slope of the flume was not adjustable as it is fixed to a moderate slope (0.003 m) to ensure water flow in the flume. Because of the relatively short flume a uniform water surface profile could not be established for the

flume inlet and outlet region. However, within the working section subcritical flow conditions were present at any stage of the hydrograph at any water depth.

In a series of test runs vertical velocity profiles were measured by a a downlooking Acoustic Doppler velocimeter (ADV), (Vectrino, Nortek AS®, accuracy ± 1%, sampling frequency 25 Hz) in the undisturbed flow ~ 30 cm upstream of the obstacle at peak flow conditions (d_w = 8 cm). The vertical measurements (z) were taken for $z/d_w = 0.2$ every 0.001 m above the bed while sampling duration was 120 s for each measurement. Raw data was post-processed applying a correlation filter (> 70%) (Goring & Nikora, 2002) and revealed the presence of boundary layer profiles for considered peak flow (Figure 2b-d).

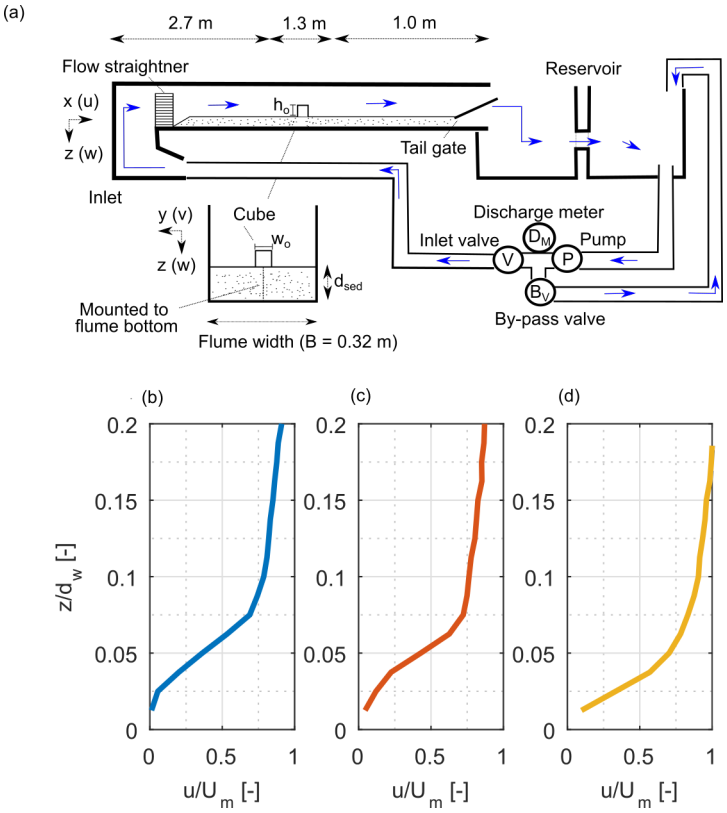

Figure 2. (a) Sketch of the flume with discharge-controlling system (arrows indicate direction of flow) and vertically measured (z –coordinate) flow profiles for longitudinal flow velocity (u).(b) U_m = 0.26 ms-1, (c) 0.32 ms^{-1}, and (d) 0.37 ms^{-1}.

2.2. Laboratory Hydrographs

Hydrographs were constructed to simulate hydrological conditions that are likely in ephemeral dryland streams (i.e. no baseflow, relatively short duration) (Camarasa-Belmonte & Segura 2001). Unsteady discharge was simulated by

a quasi steady approach applying the principle of stepped hydrographs, i.e. a sequence of constant discharges acting during defined intervals which is commonly used to imitate varying discharge in flumes (Mao 2012; López et al. 2014, Waters & Curran 2015). However, Pizarro et al., (2017) and Link et al., (2017) used a novel discharge control system able to produce complex hydrographs with continuously varying discharge in time.

Four simple shaped, and single peaked hydrographs were designed by varying the duration of rising limb (t_r), falling limb (t_f) and peak flow (t_{peak}). A symmetrical ($t_r/t_f = 1$), positive skewed ($t_r/t_f < 1$), negative skewed ($t_r/t_f > 1$), and flash flood hydrograph ($t_r/t_f \ll 1$)) were constructed by this procedure. For each hydrograph shape, three different experimental series (A, B, and C) were conducted in which the overall hydrograph duration (t_{end}) was 480 min (series A), 210 min (series B), and 120 min (series C), with $t_{end} = t_r + t_{peak} + t_f$. Thus, experimental runtime of hydrographs was not designed to define any equilibrium condition of local scouring, but to represent relative short duration hydrographs that are likely for local scouring at ephemeral conditions (i.e. Karcz, 1972, Alexander & Crooker, 2016).

For each experimental series the hydrographs were made of n = 13 intervals of constant discharge: six on the rising limb, one at peak flow, and six on the falling limb (Figure 3 a-d).

For the symmetrical hydrograph ($t_r/t_f = 1$; $t_r/t_{end} = 0.465$) of series A each interval lasted 37 min on t_r and t_f while t_{peak} lasted 36 min;

on the positive skewed hydrograph ($t_r/t_f < 1$, here = 0.28; $t_r/t_{end} = 0.2125$) the intervals on t_r and t_f lasted 17 min and 60 min, respectively, while t_{peak} lasted 18 min;

on the flash flood hydrograph ($t_r/t_f \ll 1$, here = 0.08; $t_r/t_{end} = 0.075$) the intervals on t_r and t_f lasted 6 min and 73 min, respectively, while t_{peak} lasted 6 min;

on the negative skewed hydrograph ($t_r/t_f > 1$, here = 3.53; $t_r/t_{end} = 0.75$) the intervals on t_r and t_f lasted 60 min and 17 min, respectively, while t_{peak} lasted 18 min.

Series B experiments (t_r = 1 min - 30 min, t_f = 4 min – 33 min) were designed for the positive skewed, negative skewed, and flash flood hydrograph to extent the degree of skewness of (t_r/t_f = 0.05, 0.14, and 7.06).

Series C experiments (t_r = 1 min - 15 min, t_f = 4 min – 18 min) were carried out for all hydrograph shapes.

The hydrograph started from a drained flume (i.e. no baseflow). For the rising and falling limbs of the hydrographs d_w was linearly increased from 2 cm to d_w = 8 cm at peak flow while on the falling limb d_w was decreased to 2 cm again, producing different degrees of submergence at the obstacle that were classified

based on the deformation of the water surface profile (Shamloo, 2001, Schlömer et al., 2020), (Figure 3e-f).

For unsubmerged conditions ($0 < d_w/L_o$ 1), the obstacle top was above the water surface and also a bow wave at the obstacle front could be detected, while in mid to far wake irregularities of the water surface indicate the presence of trailing vortices due to detached shear layers. Unsubmerged conditions were present for the beginning of the rising limb (i.e. interval n1 and n2) as well as for the ending of the falling limb (i.e. n12 and n13) (Figure 3e).

For shallow submergence, the obstacle top was only slightly below the water surface causing the water level to drop above the obstacle top while a bow wave piled up at the obstacle front (i.e. n3, n4 of the rising limb, and n10, n11 of the falling limb) (Figure 3f).

At full submerged conditions (d_w/L_o 2) no disturbance of the water surface profile could be observed, indicating a free flow of the approaching boundary layer above the obstacle top (i.e. n5, n6 of the rising limb, n8, n9 of the falling limb, and n7 at peak flow) (Figure 3g). However, an arch-shaped vortex might be present at the obstacle's crest and its near-wake.

Different unit discharges (q) on the intervals of the stepped hydrographs were generated by a variation of d_w and $U_{m.}$ By increasing U_m for given d_w, different flow intensities (U_m/U_c) were created that distinguish three different hydraulic scenarios. For scenario 1 clear-water conditions ($U_m/U_c < 1$) prevailed and the final value of W* ranged from 1308 to 1390 for Series A experiments depending on hydrograph shape (Figure 3h).

For scenario 2, U_m/U_c 1 and the final value of W* ranged from 6659 to 7478 for Series A experiments (Figure 3i).

For scenario 3 live-bed conditions (U_m/U_c >1) were present for the entire duration of the hydrograph and sediment was solely transported as bed load (i.e. lower stage plane bed). The flow intensity reached its maximum at peak flow. The final value of W* ranged from 26473 to 28382 for Series A experiments (Figure 3j).

For comparison, experimental runs on constant discharge at peak flow (i.e. d_w = 8, obstacle full submerged) were performed for each hydraulic scenario (i.e. U_m = 0.26 ms^{-1}, 0.32 ms^{-1}, and 0.37ms^{-1}) that lasted 480 min.

In a second experimental campaign, the impact of hydrograph chronologies (i.e. sequences of hydrographs with a certain shape) onto local scouring was evaluated by repeating the positive, negative and flash-flood hydrograph for series C (i.e. t = 120 min) for scenario 1, three times in row so that the overall runtime (t_{end}) equaled 480 min.

After each experimental run the pump was stopped and the flume was carefully drained. Afterwards, the flume was filled again to d_w = 2 cm before the pump

was started at q of the first hydrograph step. The procedure did not cause distortions of the scour hole (i.e. collapsing of scour hole flanks).

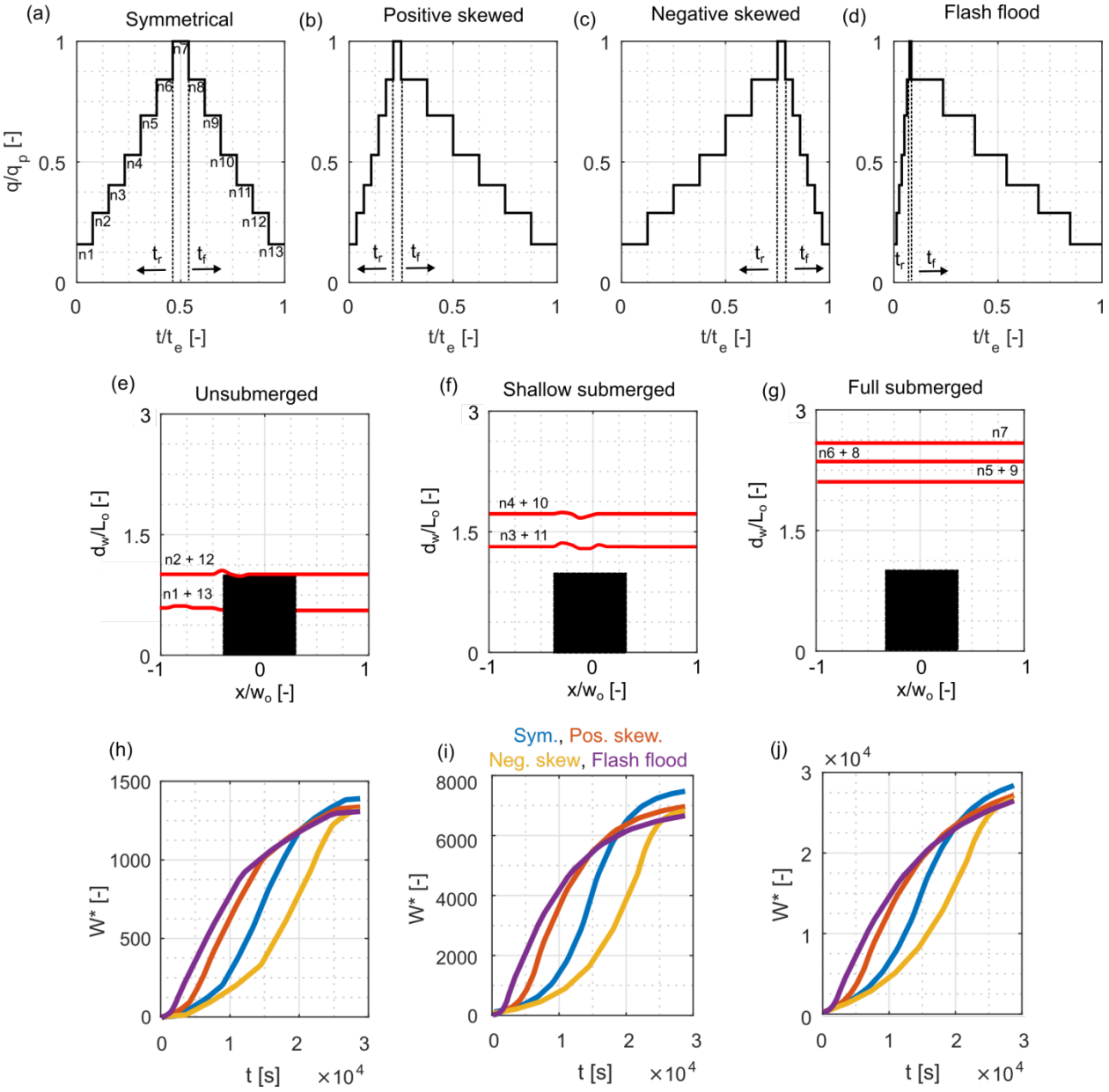

Figure 3. Laboratory hydrographs (a-c), extent of submergence at the obstacle (e-f), and dimensionless flow work (W*) over time for series A experiments.

2.3. Experimental Procedure

For each experiment q of the first interval was configured manually by adjusting the cone valves of the pump to the desired discharge while the tailgate was adjusted to d_w = 2 cm in the working section. Afterwards the obstacle was placed in the working section to start experiments at t = 0 min.

In between the intervals on the rising limb the tailgate was raised 1 to 2 cm to interrupt local scouring while q was adjusted via the cone valves of the pump to the next interval. On the falling limb, first q was decreased while the tailgate was lowered to the corresponding d_w. Adjustment of q and d_w took approximately 3 to 5 minutes and was done manually. The time of adjustment was not considered as experimental runtime as local scouring was interrupted.

Although the cone valves were operated manually, the standard error of the actual discharge was less than 9.0 *10^{-6} m^2s^{-1}, i.e. less than 3% of the desired discharge. Thus, it is argued that desired hydrographs depicted in Figure 3 are representative for actual laboratory conditions. In total 48 experimental runs were performed while hydraulic boundary conditions are displayed in Table 1.

Table 1.

Hydraulic boundary conditions of flow steps used to design hydrographs shown in Figure 3a-d

	Scen. 1[a]	Scen. 2[b]	Scen. 3[c]					
Interval (n) [-]	d_w [m]	U_c[d] [ms^{-1}]	U_m [ms^{-1}]	q [m^2s^{-1}]	U_m [ms^{-1}]	q [m^2s^{-1}]	U_m [ms^{-1}]	q [m^2s^{-1}]
+ 13				10^{-5}		10^{-5}		10^{-5}
+ 12				10^{-5}		10^{-5}		10^{-5}
+ 11				10^{-5}		10^{-5}		10^{-4}
+ 10				10^{-4}		10^{-4}		10^{-4}
+ 9				10^{-4}		10^{-4}		10^{-4}
+ 8				10^{-4}		10^{-4}		10^{-4}
				10^{-4}		10^{-4}		10^{-4}

Note. [a] A/B/C 1, 4, 7, 10. [b] A/B/C 2, 5, 8, 11. [c] A/B/C 3, 6, 9, 12. [d] Equation (11)

3 Data

The experimental dataset is accessible via the Havard dataverse repository: https://doi.org/10.7910/DVN/EYQP2U

3.1. Acquisition and Processing

The size of d_s, l_s, and w_s was measured with two LED-distance meters (Welotec®

OWRB-series, accuracy ± 0.5 mm), measuring x- and y-coordinates in a local Cartesian coordinate system, with x = longitudinal, streamwise direction and y = horizontal, perpendicular to streamwise direction. A laser distance meter (Baumer Electric® ODAM S14C, accuracy ± 1.5 mm) was used to measure the vertical coordinate (z). All sensors were mounted on a traversing system on top of the flume operating in x/y –plane. The elevation of the initial flat bed in front of the obstacle was used as reference (i.e. x0/y0/z0 = 0/0/0).

For series A, d_s, l_s, and w_s were measured every third minute on each hydrograph interval. Irrespective of time, the spatial extent of l_s and w_s was obvious and determined by $z0 < 0$. For series B and C the measurement frequency was relaxed to one and two minutes, respectively, to generate sufficient data on each hydrograph step.

However, measurements of the geometrical length scales are interpreted as quasi-dynamic observations, because they were measured while water was flowing (Rogers et al., 2020). Thus, measurements of the z-coordinate (i.e. d_s) were biased due to refraction of the laser beam within the water column. However, a simple calibration method (i.e. compensation for the travel time of light in water) yielded sufficiently accurate results when compared to measurements at drained conditions with the same measurement system (Schlömer et al. 2021). The error was less than two times D_{50}. The geometry of the local scour hole was measured by 2D cross-sectional profiles in the longitudinal i.e. streamwise direction (x/z coordinates) and horizontal i.e. perpendicular to streamwise direction (y/z coordinates) (cf. Figure 1a solid lines). Profiles were surveyed every 20 minutes of experimental runtime up to t_{end}. For the longitudinal profiles, two consecutive frontal scour profiles in time were used to estimate the volumetric bed load transport rate (qb [L^2T^{-1}]) out of the frontal scour by calculating the line integral:

$$qb\ (l_{sP}, t) \quad c^b/t_{(i+1)} - t_{(i)} \text{ [Eq. 13]}$$

with l_{sP} = longitudinal scour hole profile, c^b = depth-integrated frontal scour hole area, and i = 1, …N in which N is the total number of measured profiles in time.

In absence of suspension the sediment flux of the scour hole in terms of bed load could be estimated with an accuracy of +/- $2D_{50}$.

For further analysis qb was replaced by q* [-]:

$$q^* = qb/((\ s/\ -1)\ gD_{50}{}^3)^{1/2} \text{ [Eq. 14]}$$

Scour hole profiles were scaled with the corresponding dimensions of d_s and l_s in order to preserve collinearity of distances and angles (i.e. three or more points initially lying on a line still lie on a line after the transformation) (Tregnaghi et al. 2007).

To evaluate the impact of hydrograph sequences onto the geometry, digital elevation models (DEMs) of the scour hole after each hydrograph at drained

conditions were derived by applying Structure-from-Motion Multi-View Stereo photogrammetry (SfM-MVS) that can resolve 3-D structure from overlapping images taken from varying viewpoints (i.e. camera positions) (Westoby et al. 2012, Smith et al. 2016, Morgan et al. 2017).

Images were acquired using a Panasonic Lumix DMC-G5 (DSLM) camera with a 4/3" (17.3 x 13.0 mm), 16 megapixel image sensor and a Lumix G-Vario 14-42 mm zoom lens set at 21 mm focal length for minimal image distortion (35 mm full frame equivalent) (Javernick et al. 2014, James et al. 2019) capturing images at 4608 x 3072 pixel size at 52° field of view. The camera was mounted on a cart ~60 cm above the flume which corresponds to a ground sampling distance of 0.1 mm/pixel. By moving the cart along the longitudinal and horizontal axis of the flume, nadir imagery (i.e. pointing below a particular direction) were captured at 80% side and forward overlap over the area of interest (~ 30 x 50 cm). Additionally, images at an oblique angle (~ 45° off-nadir) were taken to enhance capturing steep features of the morphology (i.e. local scour hole). After each hydrograph a complete data set consisted of 95 images captured in 10 min. Prior to taking images, 8 Ground Control Points (GCPs) were distributed throughout the area of interest that consisted of coded circles with 4 cm diameter (Agisoft 2016). Target centroids were measured with the measurement technique described above to obtain xyz coordinates.

For the processing PhotoScan software (version 1.2.6) (Agisoft 2016) was utilized. The SfM-MVS workflow is an iterative process comprised of (i) photo alignment using a point matching algorithm that detects key points in overlapping images and solves for camera position and camera lens parameters; the alignment accuracy was set 'high' and pair selection was disabled (key point limit 40000, tie point limit 1000), identifying > 1500 key points in each photoset; (ii) georeferencing based on 2/3 of the GCPs (the remaining GCPs were used for accuracy assessment) that optimized alignment and refined camera locations by minimizing the error between modeled locations and measured locations; according to Lane et al., (2000) and James et al., (2019) the mean error (ME) was used to estimate accuracy, mean absolute error (MAE) to estimate non-directional height differences, and standard deviations (SD) to estimate precision, yielding ME = -0.003 m (x-axis), -0.001 m (y-axis), 0.001 m (z-axis); MAE = 0.005 m (x-axis), 0.003 m (y-axis), 0.0007 m (z-axis); and SD = 0.009 m (x-axis), 0.004 m (y-axis), -0.001 m (z-axis); (iii) modeling of dense point clouds based on camera locations and Multi-View Stereo reconstruction, generating dense clouds with > 8*106 points for each dataset; (iv) DEM generation based on dense point clouds at 0.2 mm/pixel (sub grain size) resolution for each dataset to enable comparison.

Geomorphic changes caused due subsequent flood events were afterward quantified by DEMs of difference. DoDs were generated using Geomorphic Change Detection software (version 7) (Wheaton et al. 2010). Thresholds of change detection (i.e. levels of detection, LoD) to evaluate uncertainty were evaluated using standard Gaussian error propagation:

$LoD = ((\ (z)_{DEM\ t1})^2 + (\ (z)_{DEM\ t2})^2)^{1/2}$ [Eq. 15]

with $(z)_{DEM\ t1}$ is the vertical error at time step 1, and $(z)_{DEM\ t2}$ is the vertical error at time step 2, respectively. Areas below LoD were considered as noise, and areas above were interpreted as topographic changes. DoDs could be constructed for a LoD = 0.1 cm.

4 Results and Discussion

4.1. Local Scour Evolution

Irrespective of hydraulic scenario and hydrograph shape local scouring immediately started after placing the obstacle in the working section at t = 0 min while the arrival of the flood front and the induced impulsive force at the obstacle did not alter the position of the obstacle.

Two initial depressions formed at the lateral edges of the obstacle front that merged to a conical scour hole in front of the obstacle (t 1 min). The position of the maximum scour depth then migrated from the lateral sides to the obstacle front. The eroded material was deposited downstream in the wake of the obstruction as a sediment ridge with orientation parallel to the flow direction. During this time the obstacle was unsubmerged (i.e. hydrograph interval n1). Thus, the observed processes are analogous to processes reported in experimental research on bridge pier scour (e.g. Escauriaza & Sotiropoulos, 2011, Bouratsis et al., 2017). At the hydrograph interval n2, d_w was equal to L_o which intensified local scouring. The scour hole significantly deepened as well as lengthened and widened the local while the sediment ridge flattened, widened and elongated in downstream direction. The intensification of local scouring processes for d_w/L_o = 1 is attributed to a high pressure gradient at the obstacle front creating an intense downflow and erosive HV-system at the obstacle base.

With increasing submergence on the rising limb of each hydrograph (i.e. interval n3 to n4) local scouring is reduced. For hydrograph intervals n6 and n6 and peak flow (n7) the obstacle was full submerged conditions (d_w/L_o 2, hydrograph intervals n5 to n6) and local scouring was considerably reduced compared to $d_w/L_o = 1$ which can be attributed to the fact (i) the majority of the approaching boundary layer flows over the obstacle and the downflow ceases, and (ii) the size and strength of the HV-system reduces as outlined by Dey et al. (2008), Sarkar (2014), and Du and Liang (2019) in experimental studies on full submerged cylinders at steady discharge.

Thus, for the present experimental series it can be stated, that peak flow does not significantly contribute to the scour hole size which is different to experimental observations reported for scouring at unsubmerged bridge piers during hydrographs (Gjunsburgs et al. 2010; Tabarestani & Zarrati 2017).

The particular importance of d_w/L_o onto local scouring becomes also obvious by considering the dimensionless flow work (W*). In Figure 4a the dimensionless scour hole depth is plotted versus W* for the symmetrical hydrograph of series

A at clear water conditions (A1) and t_{end} = 480 min. Although d_s/L_o sufficiently scales with W*, experimental data deviate from Equation (7) proposed by Pizarro et al. (2017) for unsubmerged bridge piers. This can be attributed to the aforementioned impact of d_w/L_o 2 onto local scouring during the rising limp that causes deeper scour holes at the beginning stages of the hydrograph, prior to peak flow at W* 750 (cf. Figure 3h, blue line). However, the fitting of Equation (7) is slightly better for the case of the constant A1 run for which peak flow condition prevailed during the overall duration while the obstacle was fully submerged (Figure 4a, red dots). It is worth mentioning that the size of d_s/L_o at t_{end} was comparable between A1 and the constant A1 run which highlights the importance of time onto local scouring. This becomes obvious for hydrographs C1 as the overall duration was reduced to 25% compared to series A which resulted in 12% smaller dimensionless scour hole depth irrespective of hydrograph shape (cf. Figure 4a, orange dots).

Local scour evolution was different for live-bed conditions ($U_m/U_c > 1$). For the rising limb of the symmetrical hydrograph (i.e. W* < 15000) d_s/L_o was larger compared to clear-water conditions due to higher flow intensity and sediment is mobilized from the scour hole (Figure 4b). Thus, it can be stated that for the rising limb of the hydrograph the sediment output of the scour hole is greater than the sediment input from upstream which is in accordance to previous findings reported for bridge-pier scouring (Kothyari et al. 1992b, Sheppard et al., 2006). At peak flow the sediment input from upstream reached its maximum and downstream migrating bed load sheets approached the scour hole that partially refilled and buried the local scour hole, indicated by a reduction of all geometrical length scales (i.e. d_s/L_o, l_s/L_o, w_s/L_o). At the same time the sediment output of the scour hole was reduced due to weak erosive capacity at full submerged conditions. On the falling limb slight enlargement of the local scour hole could be observed for series A and C hydrographs while for the constant run instantaneous d_s/L_o fluctuated (cf. Figure 4b).

The present observations on the size-reducing effects of passing bedload sheets onto the scour hole are in accordance with observations reported in Hong et al., (2017) on bridge pier scour affected by the passing of dune crests.

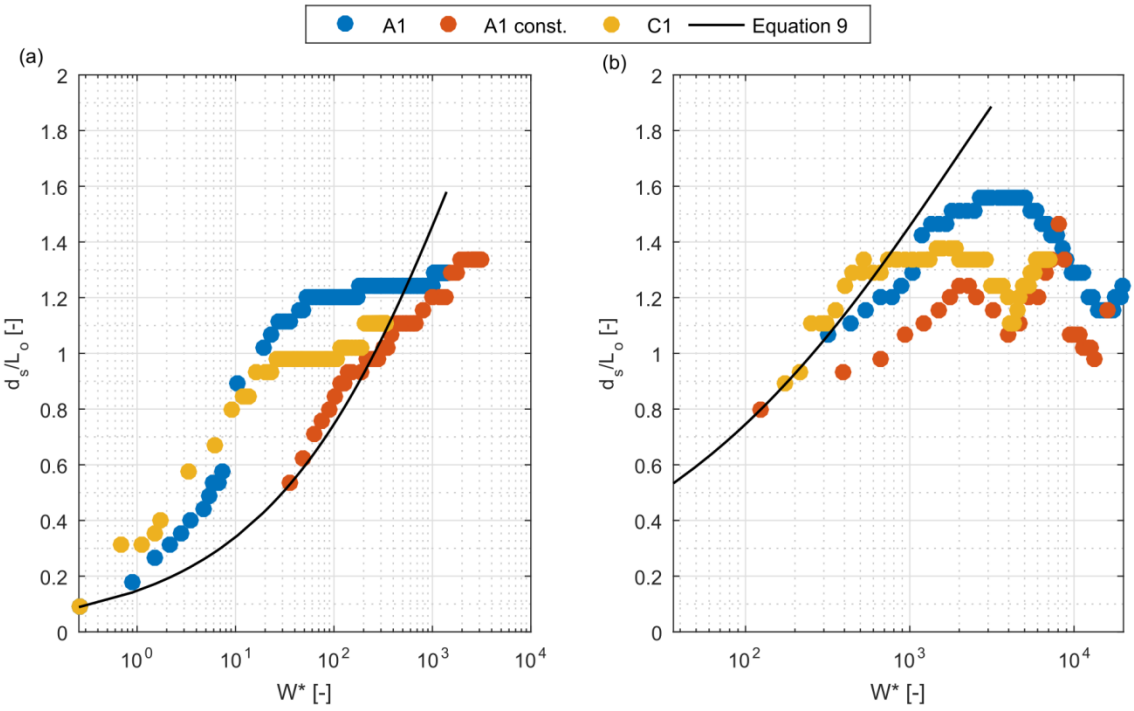

Figure 4. Dimensionless scour hole depth (d_s/L_o) observed at the symmetrical hydrograph versus dimensionless flow work (W*) for (a) clear-water conditions and (b) live-bed conditions.

The aforementioned dynamics of local scour evolution in time, i.e. intense scouring at the rising limb at d_w/L_o 1, negligible impact of peak flow due to full submergence of the obstacle, and refilling of the scour hole at live-bed conditions did not differ for different hydrograph shapes. The dimensionless bed load flux out of the scour hole (q*) was estimated by two consecutive longitudinal scour hole profiles in time (Figure 5a) and shows a non-linear evolution in time, irrespective of hydrograph shape that could be approximated by a power law relationship and ordinary least squares estimation with a mean coefficient of determination (R^2) equaling 0.83.

For clear-water conditions (Figure 5b) q* is high for the rising limb (t_r) of the hydrographs due to intense scouring and enlargement of geometrical length scales at d_w/L_o 1. Afterwards, q* significantly decreased proceeding peak flow (vertical grey lines) and reached an almost null value at the falling limb (t_f). This evolution in time was comparable for live-bed conditions (Figure 5c). An ANCOVA test (F-value = 1.32 – 1.59, p-value = 0.02) on the log-transformed values of q* and t/t_{end} revealed that q* over t/t_{end} did not statistically differ for amongst hydrograph shapes at 95% confidence interval for clear-water and

live-bed conditions.

However, for live-bed conditions q* turned negative at peak flow for each hydrograph shape as approaching bed load sheets refilled the scour hole while erosive capacity of the HV system was reduced due to full submergence of the obstacle. Afterwards, q* turns positive again, recovering to bed load comparable to q* prior to peak flow so that the scour hole reconstituted to a size comparable to pre-peak flow conditions as the sediment supply into the local scour hole mitigated.

Thus, the estimated bed load (q^b) out of the scour hole varied with unit discharge (q) on t_r and t_f irrespective of hydraulic scenario which is referred as hysteresis (Brownlie 1981).

For clear-water conditions a clockwise hysteresis pattern was present (Figure 5d) while for U_m/U_c 1 and live bed conditions ($U_m/U_c > 1$) a figure-8 hysteresis loop (Williams 1989) was present (Figure 5e). The two experimental observed hysteresis loops coincide with field observations on local scouring at logs embedded in sand and affected by different extent of submergence during flood events reported by Borg et al., (2007).

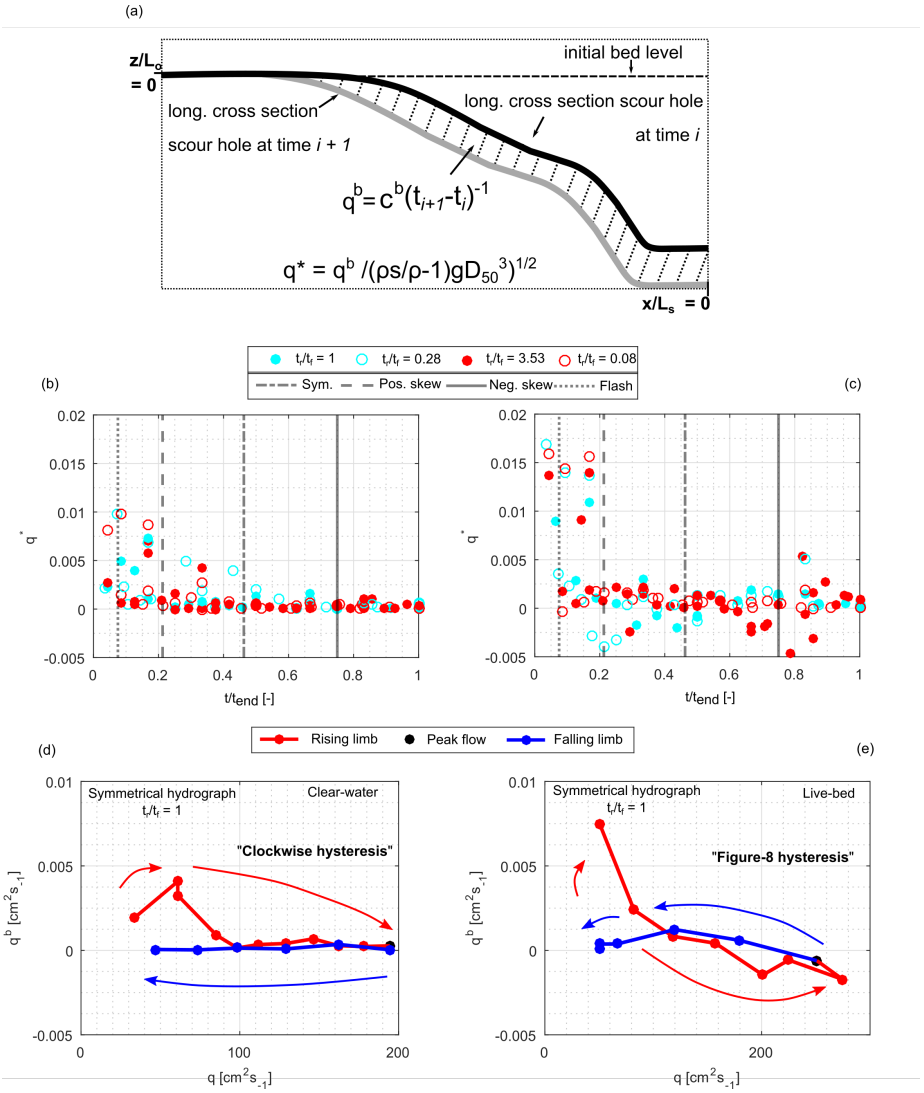

Figure 5. Estimation of bed load out of the scour hole (a). Dimensionless bed load versus dimensionless time for clear-water (b) and live-bed conditions (c) for different hydrograph shapes. Hysteresis patterns for clear-water (d) and live-bed conditions (e).

Local scouring at different hydrograph shapes at clear-water conditions showed an asymptotic evolution in time. Here, enlargement in scour depth occurred for the rising limb (t_r) prior to peak flow (q_p) irrespective of hydrograph shape, while substantial enlargement on the falling limb (t_f) was negligible (Figure 6, blue dots). For series A experiments (t_{end} = 480 min) irrespective of hydrograph shape d_s/L_o already reached 76% of its size at t_{end} at t/t_{end} = 0.1. However,

the skewness of the hydrograph (t_r/t_f) affected local scouring in time. For the negative skewed hydrograph ($t_r/t_f = 3.53$) of series A experiments, 99% of d_s/L_o at t_{end} were reached during t_r and prior to q_p (Figure 6d) while for the flash flood hydrograph ($t_r/t_f = 0.08$) 82% of d_s/L_o at t_{end} were reached during t_r which corresponds to 7.5% of the duration of t_e (Figure 6c). This observation is supported considering the two extremums of the investigation (series B, t_{end} = 210 min). For $t_r/t_f = 0.05$, 69% of d_s/L_o at t_{end} were reached during t_r while for $t_r/t_f = 7.06$, 99% of d_s/L_o at t_{end} were reached during t_r and prior to reach q_p. Thus, it can be stated that the steeper t_r (i.e. positive skewed) the quicker d_s achieves a size comparable to its final sizes for given hydraulic conditions and experimental runtime. This observation coincides with experimental results on the time evolution of d_s at bridge piers during hydrographs (Chang et al. 2004; Salamatian et al. 2014).

However, considering the symmetrical hydrograph ($t_r/t_f = 1$) it becomes obvious that especially the intervals n1 and n2 significantly contributed to an enlargement of d_s/L_o (Figure 6a, indicated by arrow). These intervals correspond to conditions for which d_w/L_o 1. Furthermore, due to increase in q and flow depth to $d_w/L_o = 1$, the superimposing of d_s/L_o , i.e. the memorization of the previous scour depth is obvious irrespective of hydrograph shape which has been also documented by Chang et al. (2004) and Hong et al (2017b) for experiments on scouring at bridge piers during unsteady flow.

For live bed conditions (Figure 6, orange dots) the skewness of the hydrograph controlled the amount of refilling of the scour hole. For $t_r/t_f = 0.08$, d_s/L_o at q_p was reduced 9% compared to its prior maximum value (Figure 6c). For t_r/t_f = 3.53 d_s/L_o at q_p was reduced 26% compared to its prior maximum value due to a larger time-span of sediment input into the scour hole (Figure 6d).

Irrespective of hydrograph shape the size of d_s/L_o at t_{end} was similar for clear-water conditions indicated by a relative standard deviation of 0.0282. For live-bed conditions the relative standard deviation was 0.0395. For all experimental series, the shape of the hydrograph did not influence the final value of d_s/L_o at the end of the experimental run which is consistent with observations reported by Link et al. (2017) on bridge pier scour.

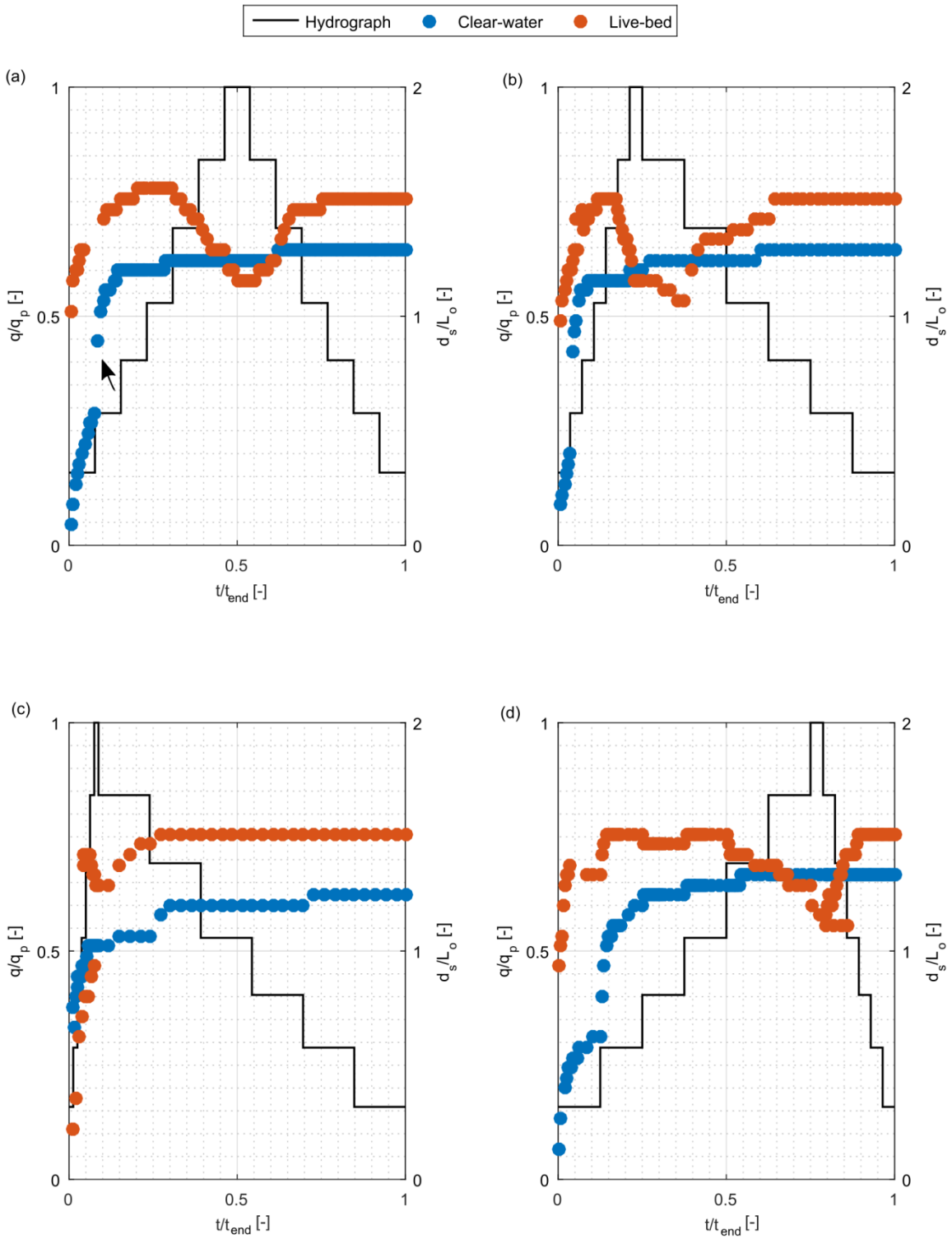
Hydrograph
Clear-water
Live-bed
(a)
(b)
(c)
(d)
q/q_p [-]
d_s/L_o [-]
t/t_end [-]
0
0.5
1
2

Figure 6. Trajectory of dimensionless scour hole depth (d_s/L_o) versus dimensionless time (t/t_e) at clear-water and live-bed conditions for series A experiments and different hydrograph shape. (a) Symmetrical. (b) Positive skewed. (c) Flash-flood. (d) Negative skewed.

4.2. Local Scour Geometry

By neglecting different hydrograph shape and duration a monotonic increase and co-variation of l_s/L_o and w_s/L_o with d_s/L_o was present for clear-water and live-bed conditions of all experimental series that could be estimated by:

$l_s/L_o = 1.79 d_s/L_o$ [Eq. 16]

with a coefficient of determination (R^2) = 0.88 (Figure 7a)

$w_s/L_o = 3.89 d_s/L_o$ [Eq. 17]

with $R^2 = 0.82$ (Figure 7b).

The enlargement of l_s and w_s was triggered by the deepening within the inner scour hole that undermined the scour slopes and induced intermittent gravitational movements at the flanks. In the developing scour holes the segmentation depicted in Figure 1b were obvious during experiments. The inclination of upper scour slope (Φ) showed a decreasing tendency in time. For t/t_{end} 0.25 Φ ranged from 32°-40° and frequent sliding of sediment could be observed while for $t/t_{end} > 0.5$ 1 Φ was 23° to 32 and gravitational movements at the slope eased. For the same time the span of the scour hole bottom (S_b) expanded from S_b/L_o 0.3 to to S_b/L_o 0.6. The enlargement of S_b is attributed to the expansion of the HV during scouring that has been documented in an experimental study on bridge pier scour reported by Guan et al. (2019). The expansion of the HV decreases the shear stress beneath the vortex for sediment mobilization and contributes to the asymptotically approaching of an equilibrium condition of scour depth (Dargahi 1990; Unger & Hager 2007).

For clear-water conditions the scaled longitudinal and horizontal profiles of the scour hole superimposed and collapsed into a narrow band irrespective of time (Figure 7c-d) which is consistent to experimental observations on scour holes at rock sills reported by Tregnaghi et al. (2007) and (2009). The evolution of the longitudinal and horizontal cross-sections of the scour hole could be modeled by Gaussian functions (Schalko et al. 2019):

$(z+d_s)/d_s = 1.037\, e^{(-((ls/x-1.7138)/0.7463)2)} + 0.6074\, e^{(-((ls/x-0.8417)/0.4782)2)}$ [Eq.18]

with $R^2 = 0.99$ (Figure 7c)

$(z+d_s)/d_s = 1.0112\ e^{(-((ws/y-1.0899/0.64412)} + 1.0086\ e^{(-((ws/y-1.1140)/0.5726)2)))}$ [Eq.19]

with $R^2 = 0.97$ (Figure 7d)

The conical shape of the shape of the scour hole remained unchanged throughout the experiments for $t > 1$ min. irrespective of clear-water or live-bed conditions

which is in agreement to experimental observations on bridge pier scour reported by Link et al. (2007). Thus, assuming the shape of an inverted frustum-cone the volume of the scour hole (V_s) could be estimated by:

$V_s = (d_s \quad / 3) (l_s^2 + S_b * l_s + S_b^2)$ [Eq.20]

For clear-water conditions and irrespective of hydrograph shape the normalized scour hole volume ($V_s/B^{1/3}$) showed reasonable agreement to an mechanistically model proposed by Schlömer et al. (2021) that assesses scour hole enlargement in time based on (i) d_s, (ii) cotangent of slope inclination ($\tan^{-1}$ (Φ)), and (iii) (S_b) (Figure 7e). The coefficient of determination (R^2) is 0.91.

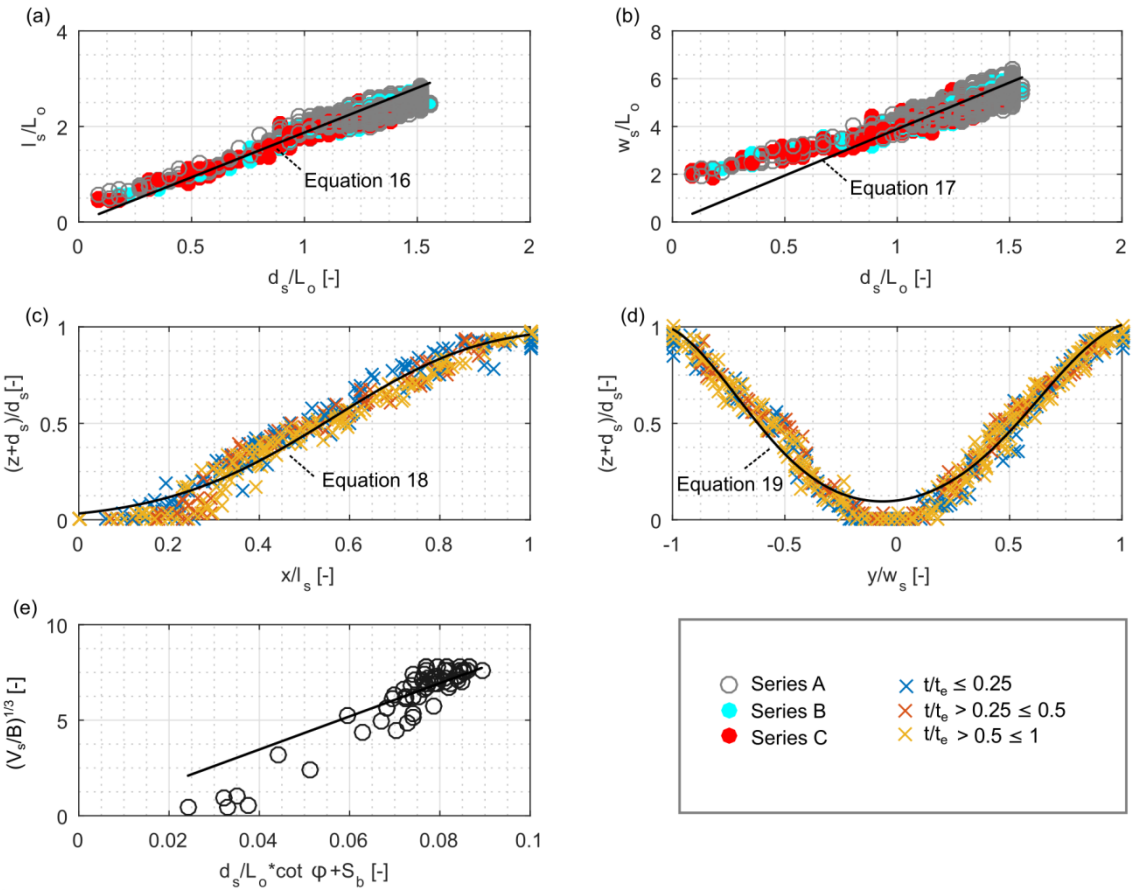

Figure 7. Relation of non-dimensional geometrical length scales of scour hole. (a) scour length. (b) scour width. (c) Scaled longitudinal and (d) horizontal scour hole profile. (e) Normalized scour hole volume vs. model of scour hole enlargement (Schlömer et al., 2021).

4.3. Geometrical Relation

The enlargement of l_s and w_s was directly coupled to the incision of d_s on t_r. However, the geometrical relations (i.e. d_s/l_s, d_s/w_s) were not constant over time. At clear-water conditions and irrespective of hydrograph shape a piecewise linear pattern is present that is composed of

1. considerable enlargement in d_s/l_s and d_s/w_s for the beginning of experiments as d_s increased quicker than l_s and w_s, approaching a maximum value in d_s/l_s and d_s/w_s;
2. easing enlargement and decreasing tendency in d_s/l_s and d_s/w_s afterwards as d_s matured to its finale size while slight enlargement in w_s occurred (Figure 8).

Quantitatively, the stages are separated by change points that mark instabilities in the slope coefficients (ß1) for the regression of d_s/l_s and d_s/w_s over t/t_e. In between the change points the slope coefficients were significantly different irrespective of hydrograph shape. Before the change point in time ß1 is » 1 which corresponds to conditions described in (i). After the change point ß1 is near zero or negative which belongs to processes formulated in (ii). Analyses to derive ß1 were performed on the de-trended data (Figure 8, grey dots).

For different hydrograph shapes at clear-water conditions the occurrence of change points in d_s/l_s over t/t_{end} slightly varied, ranging from $t/t_{end} = 0.0167$ at $t_r/t_f = 0.05 – 0.08$ to $t/t_{end} = 0.0563$ at $t_r/t_f = 3.53 – 7.06$. For d_s/w_s over t/t_e the change points occurred at $t/t_{end} = 0.0238$ to 0.175. Thus, it is proposed that two temporal stages can be described based on the geometrical relations of the local scour hole. The first stage is characterized by considerable deepening of the scour hole, the second stage is characterized by a reduced deepening while the local scour hole then widens. The presence of two stages can be explained by the expansion of the HV during scouring that reduces the erosive energy of the vortex and vice versa the potential of the HV for further deepening of the scour hole (Rogers et al. 2020; Manes & Brocchini 2015). However, the further enlargement of w_s is attributed to the convection of detached shear layers from the legs of the HV1 at the lateral sides of the obstacle that result in strong amplification of shear stress at the bed as shown by Kirkil et al. (2008) and Kirkil and Constantinescu (2010). The present observation of different stages of local scouring corresponds to results reported in Schlömer (2021) for local scouring at boulder-like obstacles exposed to long lasting (t_{end} = 5760 min) constant discharge where substantial depth-incision occurred for t/t_{end} 0.04.

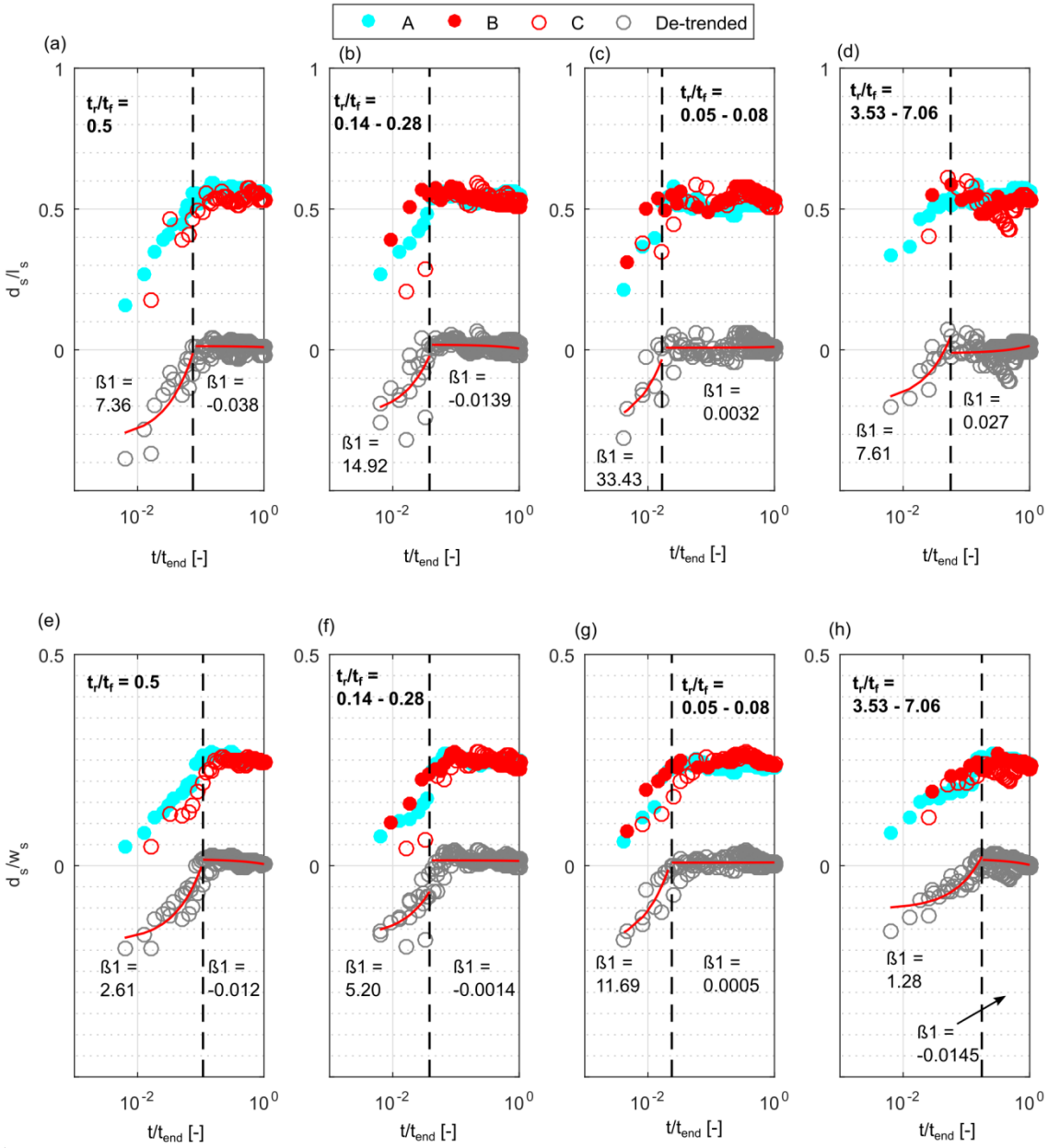

Figure 8. Geometrical relations of the scour hole vs. non-dimensional time for clear-water conditions and different hydrograph shape. (a/e) Symmetrical. (b/f) Positive skewed. (c/g) Flash-flood. (d/h) Negative skewed.

4.4. Impact of discharge chronologies

Experiments of repeated discharge events of a certain shape at clear-water conditions revealed that increment of d_s and l_s was largest for the rising limb of the first hydrograph for which 80-90 % of the dimensions at t_{end} were reached. After hydrograph II substantial enlargement of d_s and l_s was negligible and asymptotically approached its final value at $t_{end} = 480$ min irrespective of hydrograph shape. However, slight enlargement of w_s was present past hydrograph II for all considered hydrograph shapes. These results are reasoned by the modeled DEMs after each hydrograph event that is exemplified for the flash-flood hydrograph in Figure 9. The scour hole was persistent throughout the discharge events (Figure 9a-d) while considerable erosion of the entire area of the local scour hole is present for DoD 1 (Figure 9e). The amount of erosion is decreasing for DoD 2 (Figure 9f). For DoD 3 deposition is dominant due to the sediment reworking at the sediment ridge which extends in the downstream direction. The size of the geometrical length scales after hydrograph IV (i.e. 480 min) was equal to the size of d_s, l_s and w_s of series A experiments with equal experimental duration.

Although d_s, l_s, and w_s were cumulating, it becomes obvious that local scouring is an history dependent phenomenon for which a relative change in the geometrical length scales during one hydrograph event depends on d_s, l_s, and w_s reached before the occurrence of the event itself, previously described by Tubaldi et al., (2017) and Pizarro and Tubaldi (2019) as memory effect.

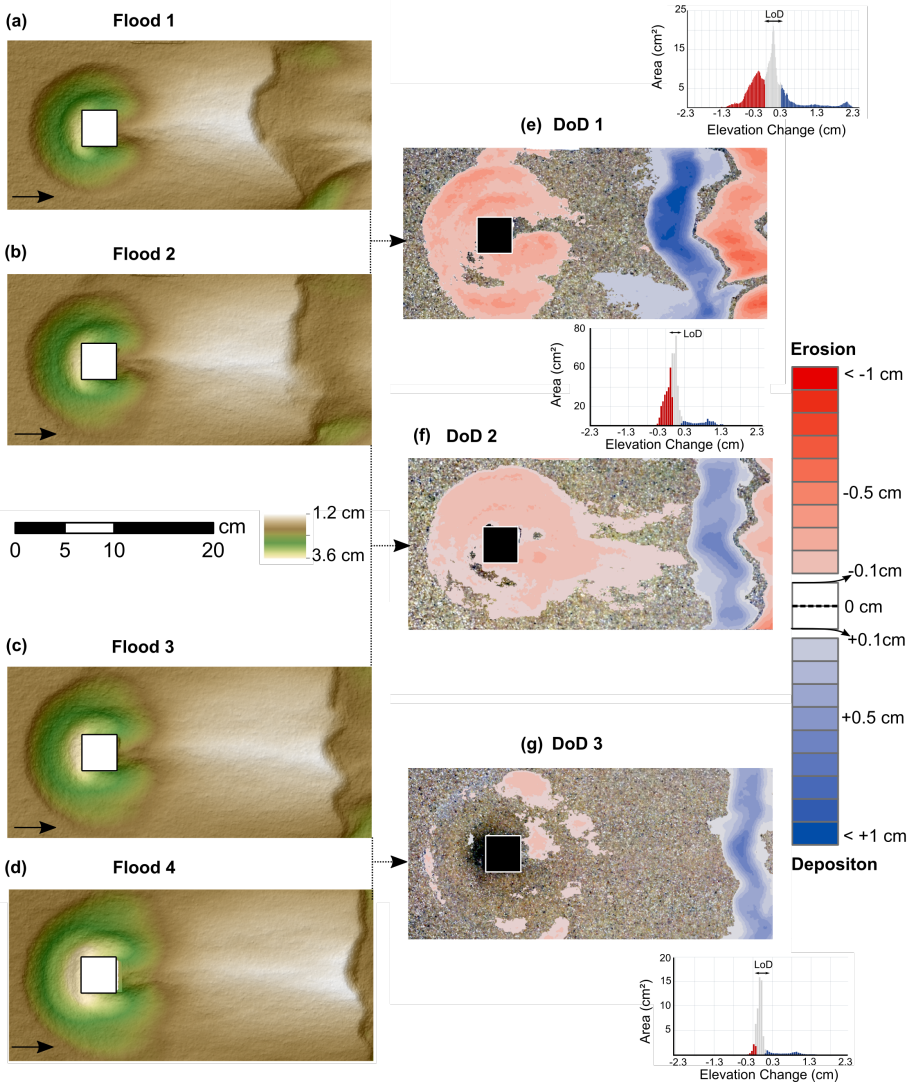

Figure 9. Modeled DEMs (a-d) and associated DoDs (e-g) for flash-flood hydrographs at clear-water conditions. Arrows indicate direction of flow.

4.5. Shortcomings of the Experimental Setup

The experimental series were conducted at reduced complexity and neglected boundary conditions of local scouring at boulder-like obstacles at field conditions that should be briefly discussed. The obstacle was not mobile. According to laboratory results presented in Schlömer et al. (2021) the movement is characterized by (i) upstream tilting of the obstacle relative to its origin position before scouring and (ii) self-burial of the obstacle i.e. reduction of h_o relative

its height before scouring. Both processes alter the obstacle's exposure to flow, and reduce the height of the obstacle protruding into flow that significantly decelerates local scouring in time and induces a near equilibrium condition earlier. The scour holes are than shallower and shorter in length compared to conditions when the obstacle is mounted.

Although live-bed conditions and refilling processes during hydrographs were considered in the present experimental series, the flow intensity ($U_m/U_c = 1.13$) is rather small compared to flow intensities likely to floods at natural conditions (U_m/U_c 20) (Ettmer et al. 2015; Link et al. 2017). Thus, the impact short-term bed degradation (i.e. Chiew, 2004, Hong et al., 2012) onto local scour hole geometry could not be addressed. However, for boulder-like obstacles it is supposed that increasing flow intensity might cause (a) an complete burial of the local scour hole due to the continuous sediment supply and the passage of bed forms; (b) a mobilization of the obstacle itself due to impulsive force that is directed from the high-pressure side of the frontal face towards the low-pressure wake and consequently lifts the obstacle (Alexander & Cooker 2016; Carling et al. 2010). Consequently, no scour hole would have formed.

5 Conclusions

Local scouring at an obstacle during unsteady discharge and variable submergence at the obstacle conditions was experimentally investigated for clear-water and live-bed conditions. The experiments were designed to mimic local scouring at boulders in ephemeral streams affected by the occurrence of flash-floods, i.e. a flow of water that arrives suddenly at a fixed point, changes rapidly in velocity and flow depth, and lasts a short time (cf. Alexander & Crooker, 2016). Although only simple shaped, single peaked hydrographs could been constructed that are in contrast to the possible infinite range of different hydrograph shapes for natural conditions, the following conclusions considering local scouring at boulders in ephemeral streams are drawn:

1. Up to 85% of scouring was observed on the rising limb of the hydrographs when flow depth (d_w) is comparable to the size of the obstacle (L_o), i.e. d_w/L_o 1. The obstacle than is unsubmerged which has paramount impact for the size of the emerging scour hole in depth (d_s), length (l_s) and width (w_s), because an intense downflow at the obstacle front is present due to an high pressure gradient that in addition to an strong horseshoe vortex system (HV) at the obstacle base favors scouring processes. Similar conditions are described for scouring at bridge piers (cf. Melville & Coleman, 2000). With increasing submergence in the course of the hydrograph ($d_w/L_o > 1$) locals scouring eases the downflow while also the HV weakens. Thus, it is supposed that in dependence of flow depth the peak flow of a flood might only marginal impact the size of the local scour hole if the obstacle is fully submerged, which is in contrast to bridge pier scouring.

2. The size of the scour holes at boulder-like obstacles scales with the dimensional flow work of the hydrograph, proposed by Pizarro et al., (2017).

3. Up to 80% of the scour hole size at the end of experimental runs was reached in only 10% of the experimental runtime while the shape of a hydrograph in terms of its skewness played an important factor. The steeper the rising limb the quicker the size of d_s, l_s, and w_s matured. The enlargement of l_s, and w_s is therefore attributed to the deepening of the scour hole that undermined the scour slopes and induced gravitational movements. A simple mechanistically model is presented that assesses scour hole volume in time based on scour depth, the inclination of the scour hole slopes, and the span of the scour hole bottom

   Moreover, two temporal evolution stages of the local scour hole are identified based on its geometrical relations (d_s/w_s, d_s/l_s). It is speculated that the geometrical relation of preserved local scour holes at boulder obstacles located in ephemeral streams may be used as length scale to plausible estimate the minimum duration of the rising limb of a flood hydrograph.

1. Experimental runs on the impact of discharge chronologies at clear-water conditions revealed that local scour holes are transient bed features in the sense that they persist as long as the obstacles that create them are present. However, boulders are mobile and scouring causes tilting and self-burial of the obstacle. Additionally, live-bed conditions during floods and the passage of bedforms might cause a disappearance of the structure

2. Local scouring is history dependent at subsequent hydrograph events and memory effects are present that describe the dependence on antecedent sizes of d_s, l_s, and w_s. The greatest impact on the size of the scour hole is attributed to the rising limb of the initial hydrograph event for which 80-90 % of the dimension at the end of the experiments were attained.

Acknowledgments

The present study was not financially supported.

Open Research

The data presented here can be downloaded in tabular form on condition that we are acknowledged in any subsequent publication.

References

Agisoft (2016): Agisoft PhotoScan User Manual. Professional edition, Version 1.2. https://www.agisoft.com/pdf/photoscan-pro_1_2_en.pdf. Accessed 19 May 2021.

Alexander, J, & Cooker, M. J. (2016): Moving boulders in flash floods and estimating flow conditions using boulders in ancient deposits. Sedimentology 63 (6), 1582–1595, https://doi.org/10.1111/sed.12274

Allen J. R. L. 1984. *Sedimentary structures: Their character and physical basis.* Amsterdam, Elsevier.

Baynes, E R.C., van de Lageweg, W. I., McLelland, S. J., Parsons, D. R., Aberle, J., Dijkstra, J. et al. (2018): Beyond equilibrium: Re-evaluating physical modelling of fluvial systems to represent climate changes. *Earth-Science Reviews* 181, 82–97, https://doi.org/10.1016/j.earscirev.2018.04.007

Bombar, G. (2020): Scour Evolution Around Bridge Piers Under Hydrographs with High Unsteadiness. *Iranian Journal of Science and Technology Transactions of Civil Engineering* 44 (1), 325–337, https://doi.org/10.1007/s40996-019-00321-8

Bouratsis P, Diplas P, Dancey CL, Apsilidis N. 2017. Quantitative Spatio-Temporal Characterization of Scour at the Base of a Cylinder. *Water* 9(3): 227 https://doi.org/10.3390/w9030227

Boyer C., Roy A.G. (1991): Morphologie du lit autour d'un obstacle soumis à un écoulement en couche mince. *Géographie physique et Quaternaire* 45 (1): 91–99,

Breusers, H. N. C., & Raudkivi, A. J. (1991): *Scouring* (Hydraulic structures design manual, 2) Rotterdam: Balkema

Brownlie, W. R. (1981): Prediction of flow depth and sediment discharge in open channels, Report KH-R-43A Pasadena: California Institute of Technology

Calle, M., Alho, P., Benito, G. (2017): Channel dynamics and geomorphic resilience in an ephemeral Mediterranean river affected by gravel mining. *Geomorphology* 285, 333-346, http://dx.doi.org/10.1016/j.geomorph.2017.02.026

Camarasa-Belmonte, A M., & Segura, F. (2001): Flood events in Mediterranean ephemeral streams (ramblas) in Valencia region, Spain. *CATENA* 45 (3), 229–249, https://doi.org/10.1016/S0341-8162(01)00146-1

Carling, P. A., Hoffmann, M., Blatter, A. S. (2010): Initial Motion of Boulders in Bedrock Channels. In P. K. House, R.H. Webb, V.R. Baker, D.R. Levish (Eds), *Ancient floods, modern hazards. Principles and applications of paleoflood hydrology* (Water Science and Application 5, pp. 147–160). Washington, DC: American Geophysical Union

Chang, W.-Y., Lai, J.-S., Yen, C.-L. (2004): Evolution of Scour Depth at Circular Bridge Piers. *Journal of Hydraulic Engineering*130 (9), 905–913, https://doi.org/10.1061/(ASCE)0733-9429(2004)130:9(905)

Chen, Y., Yang, Z., Wu, H. (2019): Evolution of Turbulent Horseshoe Vortex System in Front of a Vertical Circular Cylinder in Open Channel. *Water* 11 (10), 2079, https://doi.org/10.3390/w11102079

Chen, Q., Qi, M., Zhong, Q., Li, D. (2017): Experimental study on the multimodal dynamics of the turbulent horseshoe vortex system around a circular cylinder. *Physics of Fluids* 29 (1), 15106, https://doi.org/10.1063/1.4974523

Chiew, Y.M. (2004): Local Scour and Riprap Stability ar Bridge Piers in a Degrading Channel. *Journal of Hydraulic Engineering* 130 (3) , 218–226,

https://doi.org/10.1061/(ASCE)0733-9429(2004)130:3(218)

Chreties C., Simarro, G., Teixeira, L. (2008): New Experimental Method to Find Equilibrium Scour at Bridge Piers. *Journal of Hydraulic Engineering* 134 (10), 1491–1495, https://doi.org/10.1061/(ASCE)0733-9429(2008)134:10(1491)

Collischonn, W., Fleischmann, A., Paiva, R. C. D., Mejia, A. (2017): Hydraulic Causes for Basin Hydrograph Skewness. *Water Resources Research*53 (12), 10603–10618, https://doi.org/10.1002/2017WR021543

Comiti F., Andreoli A., Lenzi M.A. (2005): Morphological effects of local scouring in step–pool streams. *Earth Surface Processes and Landforms* 30 (12): 1567–1581, https://doi.org/10.1002/esp.1217

Dargahi, B. (1990): Controlling Mechanism of Local Scouring. *Journal of Hydraulic Engineering*116 (10), 1197–1214, https://doi.org/10.1061/(ASCE)0733-9429(1990)116:10(1197)

Dey, S. (2014): *Fluvial hydrodynamics: Hydrodynamic and sediment transport*. Berlin: Springer.

Dey, S., Sarkar, S., Bose, S.K., Tait, S., Castro-Orgaz, O. (2011), Wall-wake flows downstream of a sphere placed on a plane rough-wall, *Journal of Hydraulic Engineering* 137 (10), 1173-1189, DOI: 10.1061/(ASCE)HY.1943-7900.0000441

Dey S, Raikar R.,V, Roy A. (2008): Scour at Submerged Cylindrical Obstacles under Steady Flow. *Journal of Hydraulic Engineering* 134(1), 105–109, https://doi.org/10.1061/(ASCE)0733-9429(2008)134:1(105)

Douglas J.F., Gasiorek J.M., Swaffield J.A. (2001): *Fluid mechanics*. Prentice Hall: Harlow.

Du, S., Liang, B. (2019): Comparisons of local scouring for submerged square and circular cross-section piles in steady current. *Water* 11 (9), 1820, https://doi.org/10.3390/w11091820.

Escauriaza, C., & Sotiropoulos, F. (2011): Initial stages of erosion and bed form development in a turbulent flow around a cylindrical pier. *Journal of Geophysical Research* 116 (F3), 671, https://doi.org/10.1029/2010JF001749

Ettema, R., Constantinescu, G., Melville, B. (2011): *Evaluation of Bridge Scour Research: Pier Scour Processes and Predictions*. Washington, D.C.: Transportation Research Board.

Ettmer, B., Orth, F., Link, O. (2015): Live-Bed Scour at Bridge Piers in a Lightweight Polystyrene Bed. *Journal of Hydraulic Engineering*141 (9), 4015017, https://doi.org/10.1061/(ASCE)HY.1943-7900.0001025

Euler, Th., & Herget, J. (2012): Controls on local scour and deposition induced by obstacles in fluvial environments. *CATENA* 91, 35–46, https://doi.org/10.1016/j.catena.2010.11.002

Euler, Th., Herget, J., Schlömer, O., Benito, G. (2017): Hydromorphological processes at submerged solitary boulder obstacles in streams. *CATENA* 157, 250–https://doi.org/10.1016/j.catena.2017.05.028

Fisher A.C., Klingman P.C. (1984): Local Scour at Fish Rocks. In Schreiber D.L. (Ed). *Water for resource development: Proceedings of the Conference* (pp. 286-290). New York: ASCE

Friedrichs C.T., Rennie S.E., Brandt A. (2016): Self-burial of objects on sandy bed by scour: A synthesis of observations. In Harris J, Whitehouse R, Moxon S (eds.), *Scour and erosion: Proceedings of the 8th International Conference on Scour and Erosion, Oxford, UK, 12-15 September 2016* (pp. 179–189), CRC Press: Boca Raton

Gjunsburgs, B., Jaudzems, G., Govša, J. (2010): Hydrograph Shape Impact on the Scour Development with Time at Engineering Structures in River Flow. *Construction Science* 11, 6–12

Goring D.G, Nikora V.I. (2002): Despiking Acoustic Doppler Velocimeter Data. *Journal of Hydraulic Engineering* 128 (1): 117–126, https://doi.org/10.1061/(ASCE)0733-9429(2002)128:1(117)

Hajimirzaie S.M., Tsakiris A.G., Buchholz J.H.J., Papanicolaou A.N. (2014): Flow characteristics around a wall-mounted spherical obstacle in a thin boundary layer. *Experiments in Fluids* 55 (6): 565, https://doi.org/10.1007/s00348-014-1762-0

Herget, J., Euler, Th., Roggenkamp, Th., Zemke, J. (2013): Obstacle marks as palaeohydraulic indicators of Pleistocene megafloods. *Hydrology Research* 44 (2), 300–317, https://doi.org/10.2166/nh.2012.155

Herget, J., Schütte, F., Klosterhalfen, A. (2015): Empirical modelling of outburst flood hydrographs. *Zeitschrift für Geomorphologie Supplementary Issues* 59 (3), 177–198, https://doi.org/10.1127/zfg_suppl/2015/S-59224

Hong, J.-H., Chiew, Y.-M., Yeh, P.-H., Chan, H.-C. (2017): Evolution of Local Pier-Scour Depth with Dune Migration in Subcritical Flow Conditions. *Journal of Hydraulic Engineering*143 (4), 4016098, https://doi.org/10.1061/(ASCE)HY.1943-7900.0001261

Hong, J.-H, Raikar, R.,V., Deshmunkh, A.,R., Guo W.-D. (2017b): Scour Around Bridge Abutments under Unsteady Flow. Paper presented at 37th IAHR World Congress, Kuala Lumpur, Malaysia.

Hong, J.-H., Chiew, Y.-M., Lu, J.-Y., Lai, J.-S. (2012): Houfeng Bridge Failure in Taiwan. *Journal of Hydraulic Engineering* 138 (2), 186–198, https://doi.org/10.1061/(ASCE)HY.1943-7900.0000430

James, M., R., Chandler, J., H., Eltner, A., Fraser, C., Miller, P., E., Mills, J., P., et al. (2019): Guidelines on the use of structure-from-motion photogrammetry

in geomorphic research. *Earth Surface Processes and Landforms* 44, 20812084, https://doi.org/10.1002/esp.4637

Javernick, J., Brasington, J., Caruso, B. (2014): Modeling the topography of shallow braided rivers using Structure-from-Motion photogrammetry. *Geomorphology* 213, 166-182, https://doi.org/10.1016/j.geomorph.2014.01.006

Jomaa S., Barry D.A., Heng B.C.P., Brovelli A., Sander G.C., Parlange J.-Y. (2012): Influence of rock fragment coverage on soil erosion and hydrological response: Laboratory flume experiments and modeling. *Water Resources Research* 48 (5), https://doi.org/10.1029/2011WR011255

Karcz I. (1972): Sedimentary structures formed by flash floods in southern Israel. *Sedimentary Geology* 7 (3): 161–182, https://doi.org/10.1016/0037-0738(72)90001-2

Kirkil G., Constantinescu G. (2015): Effects of cylinder Reynolds number on the turbulent horseshoe vortex system and near wake of a surface-mounted circular cylinder. *Physics of Fluids* 27(7), 75102, https://doi.org/10.1063/1.4923063

Kirkil, G., Constantinescu, G. (2010): Flow and turbulence structure around an in-stream rectangular cylinder with scour hole. *Water Resources Research* 46 (11), https://doi.org/10.1029/2010WR009336

Kirkil G., Constantinescu S.G., Ettema R. (2008): Coherent Structures in the Flow Field around a Circular Cylinder with Scour Hole. *Journal of Hydraulic Engineering* 134 (5): 572–587, https://doi.org/10.1061/(ASCE)0733-9429(2008)134:5(572)

Kothyari, U. C., Garde, R. C. J., Kittur, G. R. R. (1992a): Temporal Variation of Scour Around Circular Bridge Piers. *Journal of Hydraulic Engineering118* (8), 1091–1106, https://doi.org/10.1080/00221689209498889

Kothyari, U. C., Ranga Raju, K. G., Garde, R. C. J. (1992b): Live-Bed Scour around Cylindrical Bridge Piers. *Journal of Hydraulic Research* 30 (5), 701–715, https://doi.org/10.1061/(ASCE)0733-9429(1992)118:8(1091)

Lane, S. N., James, T. D., Crowell, M. D. (2000): Application of digital photogrammetry to complex topography for geomorphological research. *Photogrammetric Record* 16 (95), 793-821, https://doi.org/10.1111/0031-868X.00152

Li, J., Qi, M., Fuhrman, D. R., Chen, Q. (2018): Influence of turbulent horseshoe vortex and associated bed shear stress on sediment transport in front of a cylinder. *Experimental Thermal and Fluid Science* 97, 444–457, https://doi.org/10.1016/j.expthermflusci.2018.05.008

Link, O., García, M., Pizarro, A., Alcayaga, H., Palma, S. (2020): Local Scour and Sediment Deposition at Bridge Piers during Floods. *Journal of Hydraulic Engineering146* (3), 4020003, https://doi.org/10.1061/(ASCE)HY.1943-7900.0001696

Link, O., Castillo, C., Pizarro, A., Rojas, A., Ettmer, B., Escauriaza, C., Manfreda, S. (2017): A model of bridge pier scour during flood waves. *Journal of Hydraulic Research* 55 (3), 310–323, https://doi.org/10.1080/00221686.2016.1252802

Link, O., González, C., Maldonado, M., Escauriaza, C. (2012): Coherent structure dynamics and sediment particle motion around a cylindrical pier in developing scour holes. *Acta Geophysica.* 60 (6), 1689–1719, https://doi.org/10.2478/s11600-012-0068-y

Link O., Pfleger F., Zanke U. (2008): Characteristics of developing scour-holes at a sand-embedded cylinder. *International Journal of Sediment Research* 23 (3): 258–266, https://doi.org/10.1016/S1001-6279(08)60023-2

López, G., Teixeira, L., Ortega-Sánchez, M., Simarro, G. (2014): Estimating Final Scour Depth under Clear-Water Flood Waves. *Journal of Hydraulic Engineering* 140 (3), 328–332, https://doi.org/10.1061/(ASCE)HY.1943-7900.0000804

Manes, C., Coscarella, F., Rogers, A., Gaudio, R. (2018): Viscosity effects on local scour around vertical structures in clear-water conditions. *E3S Web of Conferences.* 40, 3038, https://doi.org/10.1051/e3sconf/20184003038.

Manes, C., & Brocchini, M. (2015): Local scour around structures and the phenomenology of turbulence. *Journal of Fluid Mechanics* 779, 309–324, https://doi.org/10.1017/jfm.2015.389

Mao, L. (2012): The effect of hydrographs on bed load transport and bed sediment spatial arrangement. *Journal of Geophysical Research* 117 (F3), https://doi.org/10.1029/2012JF002428

Melville, B. W., & Chiew, Y.-M. (1999): Time Scale for Local Scour at Bridge Piers. *Journal of Hydraulic Engineering*125 (1), 59–65, https://doi.org/10.1061/(ASCE)0733-9429(1999)125:1(59)

Melville, B. W., Coleman, S. E. (2000): *Bridge scour.* Highlands Ranch, Colorado: Water Resources Publication.

Morgan J. A., Brogan D., J., Nelson, P. A. (2017): Application of Structure-from-Motion photogrammetry in laboratory flumes. *Geomorphology* 276, 125–143, https://doi.org/10.1016/j.geomorph.2016.10.021

Nakagawa, H., & Nezu, I. (1993): *Turbulence in Open Channel Flows*, Rotterdam: CRC Press.

Okamoto, S., Sunabashiri, Y. (1992): Vortex shedding from a circular cylinder of finite length

placed on a ground plane. *Journal of Fluids Engineering* 114 (4): 512-521, https://doi.org/10.1115/1.2910062

Oliveto, G., Hager, W. H. (2002): Temporal Evolution of Clear-Water Pier and Abutment Scour. *Journal of Hydraulic Engineering128* (9), 811–820, https:

//doi.org/10.1061/(ASCE)0733-9429(2002)128:9(811)

Paik J., Escauriaza C., Sotiropoulos F. (2007): On the bimodal dynamics of the turbulent horseshoe vortex system in a wing-body junction. *Physics of Fluids* 19 (4): 45107, https://doi.org/10.1063/1.2716813

Pagliara S., Palermo M. (2018): Equilibrium scour morphology downstream of rock sills under unsteady flow conditions. *E3S Web of Conferences* 40: 3004, https://doi.org/10.1051/e3sconf/20184003004

Pagliara S., Palermo M. (2008): Scour control and surface sediment distribution downstream of block ramps. *Journal of Hydraulic Research* 46 (3): 334–343, https://doi.org/10.3826/jhr.2008.3208

Pattenden R.J., Turnock S.R., Zhang X. (2005): Measurements of the flow over a low-aspect-ratio cylinder mounted on a ground plane. *Experiments in Fluids* 39 (1): 10–21, https://doi.org/10.1007/s00348-005-0949-9

Papanicolaou A.N., Kramer C.M., Tsakiris A.G., Stoesser T., Bomminayuni S., Chen Z. (2012): Effects of a fully submerged boulder within a boulder array on the mean and turbulent flow fields: Implications to bedload transport. *Acta Geophysica* 60(6), 1502–1546, https://doi.org/10.2478/s11600-012-0044-6

Papanicolaou, A. N., Tsakiris A.G., Kramer C.M. (2010): Effects of relative submergence on flow and sediment patterns around clasts. In *River Flow 2010 (pp.* 793–799). Karlsruhe, Germany: Bundesanstalt für Wasserbau.

Pizarro, A., Manfreda, S., Tubaldi, E. (2020): The Science behind Scour at Bridge Foundations: A Review. *Water* 12 (2), 374, https://doi.org/10.3390/w12020374

Pizarro A., Tubaldi E. (2019): Quantification of Modelling Uncertainties in Bridge Scour Risk Assessment under Multiple Flood Events. *Geosciences* 9 (10), 445, https://doi.org/10.3390/geosciences9100445

Pizarro, A., Ettmer, B., Manfreda, S., Rojas, A., Link, O. (2017): Dimensionless Effective Flow Work for Estimation of Pier Scour Caused by Flood Waves. *Journal of Hydraulic Engineering*143 (7), 6017006, https://doi.org/10.1061/(ASCE)HY.1943-7900.0001295

Poesen J.W., Torri D., Bunte K. (1994): Effects of rock fragments on soil erosion by water at different spatial scales: a review. *CATENA* 23(1-2): 141–166, https://doi.org/10.1016/0341-8162(94)90058-2

Polvi, L.E. (2021): Morphodynamics of boulder-bed semi-alluvial streams in northern Fennoscandia: a flume experiment to determine sediment self-organization. Water Resources Research 57 (3), e2020WR028859, https://doi.org/10.1029/2020WR028859

Powell, D. M. (2009): Dryland rivers: processes and forms. In A.J. Parsons & A D. Abrahams (Eds.): *Geomorphology of Desert Environments* (pp. 333-373). Dordrecht: Springer.

Radice, A., Porta, G., Franzetti, S. (2009): Analysis of the time-averaged properties of sediment motion in a local scour process. *Water Resources Research* 45 (3), https://doi.org/10.1029/2007WR006754

Radice, A., & Tran, C. K. (2012): Study of sediment motion in scour hole of a circular pier. *Journal of Hydraulic Research* 50 (1), 44–51, https://doi.org/10.1080/00221686.2011.641764

Reid, I., Laronne, J. B., Powell, D. M. (1998): Flash-flood and bedload dynamics of desert gravel-bed streams. *Hydrological Processes* 12 (4), 543–557, https://doi.org/10.1002/(SICI)1099-1085(19980330)12:4<543::AID-HYP593>3.0.CO,2-C

Rennie, S. E., Brandt, A., Friedrichs, C. T. (2017): Initiation of motion and scour burial of objects underwater. *Ocean Engineering* 131, 282–294, https://doi.org/10.1016/j.oceaneng.2016.12.029

Richardson, P., D. (1968): The generation of scour marks near obstacles. *Journal of Sedimentary Research* 38 (4), 965–970, https://doi.org/10.1306/74D71AD7-2B21-11D7-8648000102C1865D

Rogers, A., Manes, C., Tsuzaki, T. (2020): Measuring the geometry of a developing scour hole in clear-water conditions using underwater sonar scanning. *International Journal of Sediment Research* 35 (1), 105–114, https://doi.org/10.1016/j.ijsrc.2019.07.005

Salamatian, A., Tabarestani, M. K., Zarrati, A. R. (2014): Local scour at cylindrical bridge pier under a flood wave. In *River Flow 2014* (pp. 1387–1391) Leiden: CRC Press.

Sarkar A. (2014): Scour and flow around submerged structures. *Proceedings of the Institution of Civil Engineers - Water Management* 167(2): 65–78, https://doi.org/10.1680/wama.12.00117

Schalko, I., Lageder, C., Schmocker, L., Weitbrecht, V., Boes, R. M. (2019): Laboratory Flume Experiments on the ormation of Spanwise Large Wood Accumulations: Part II – Effect on local scour. Water Resources Research 55 (6), 4871–4885, https://doi.org/10.1029/2018WR024649

Schlömer, Oliver (2020): Morphodynamic relation of obstacle marks at boulder-like obstructions in time. In Uijttewaal, W., Franca M.J., Valero D., Chavarrias, V., Ylla Arbós, C., Schielen, R., Crosato, A. (Eds.) River Flow 2020. (pp. 719-727) Leiden: CRC Press.

Schlömer, O., Herget, J., Euler, Th. (2020): Boundary condition control of fluvial obstacle mark formation – framework from a geoscientific perspective. Earth Surface Processes and Landforms 45 (1), 189–206, https://doi.org/10.1002/esp.4793

Schlömer, O., Grams, P. E., Buscombe, D., Herget, J. (2021): Geometry of obstacle marks at instream boulders – integration of laboratory investigations

and field observations. *Earth Surface Processes and Landforms* 46 (3), 659679, https://doi.org/10.1002/esp.5055

Shamloo, H., Rajaratnam, N., Katopodis, C. (2001): Hydraulics of simple habitat structures. *Journal of Hydraulic Research* 39 (4), 351–366, https://doi.org/10.1080/00221680109499840

Sheppard, D. M., & Miller, W. (2006): Live-Bed Local Pier Scour Experiments. *Journal of Hydraulic Engineering*132 (7), 635–642, https://doi.org/10.1061/(ASCE)0733-9429(2006)132:7(635)

Shobe, C. M., Turowsi, J. M., Nativ, R., Glade, R. C., Bennett, G. L., Dini, B. (2021): The role of infrequently mobile boulders in modulating landscape evolution and geomorphic hazards. *Earth-Science Reviews* 220, 103717, https://doi.org/10.1016/j.earscirev.2021.103717

Simarro, G., Fael, C. M. S., Cardoso, A. H. (2011): Estimating Equilibrium Scour Depth at Cylindrical Piers in Experimental Studies. *Journal of Hydraulic Engineering* 137 (9), 1089–1093, https://doi.org/10.1061/(ASCE)HY.1943-7900.0000410

Simarro, G., Teixeira, L., Cardoso, A. H. (2007): Flow Intensity Parameter in Pier Scour Experiments. *Journal of Hydraulic Engineering* 133 (11), 1261–1264, https://doi.org/10.1061/(ASCE)0733-9429(2007)133:11(1261)

Simons D.B., Richardson E.V. (1966): Resistance to flow in alluvial channels: US Geological Survey Professional Paper 422-J: Washington.

Sonin A.A. (2004): A generalization of the -theorem and dimensional analysis. *PNAS* 101 (23), 8525-8526, https://doi.org/10.1073/pnas.0402931101

Smith, M. W., Carrivick, J., L., Quincey, D. J. (2016): Structure from motion photogrammetry in physical geography. *Progress in Physical Geography* 40 (2), 247275, https://doi.org/10.1177/0309133315615805

Sumer B.M., Fredsøe J. (2005): *The mechanics of scour in the marine environment*. World Scientific Publication: New Jersey.

Tabarestani, M. K., Zarrati, A. R. (2017): Local scour calculation around bridge pier during flood event. *KSCE Journal of Civil Engineering* 21 (4), 1462–1472, https://doi.org/10.1007/s12205-016-0986-3

Tregnaghi M., Marion A., Gaudio R. (2007). Affinity and similarity of local scour holes at bed sills. *Water Resources Research* 43(11): W11417, https://doi.org/10.1029/2006WR005559

Tregnaghi M., Marion A., Coleman, S. (2009): Scouring at Bed Sills as a Response to Flash Floods. Journal of Hydraulic Engineering 135 (6), 466–475, https://doi.org/10.1061/(ASCE)HY.1943-7900.0000033

Tubaldi, E., Macorini, L., Izzuddin, B. A., Manes, C., Laio, F. (2017): A framework for probabilistic assessment of clear-water scour around bridge piers. *Struc-*

tural Safety 69, 11–22, https://doi.org/10.1016/j.strusafe.2017.07.001

Unger, J., & Hager, W. H. (2007): Down-flow and horseshoe vortex characteristics of sediment embedded bridge piers. *Experiments in Fluids* 42 (1), 1–19, https://doi.org/10.1007/s00348-006-0209-7

Waters, K. A., & Curran, J (2015): Linking bed morphology changes of two sediment mixtures to sediment transport predictions in unsteady flows. *Water Resources Research* 51 (4), 2724–2741, https://doi.org/10.1002/2014WR016083

Wheaton, J. M., Brasington, J., Darby, S. E., Sear, D. A. (2010): Accounting for uncertainty in DEMs from repeat topographic surveys: improved sediment budgets. *Earth Surface Proceses and Landforms* 35 (2), 136-156, https://doi.org/10.1002/esp.1886

Westoby M.J., Brasington J., Glasser N.F., Hambrey M.J., Reynolds J.M. (2012): 'Structure-from-Motion' photogrammetry: a low-cost, effective tool for geoscience applications. *Geomorphology* 179: 300–314, https://doi.org/10.1016/j.geomorph.2012.08.021.

Williams, G., P. (1989): Sediment concentration versus water discharge during single hydrologic events in rivers. *Journal of Hydrology* 111 (1-4), 89106, https://doi.org/10.1016/0022-1694(89)90254-0